Theses and Dissertations

May 2018

Examining Urban Heat Island Effect and Its Public Health Implications with Remotely Sensed Data

Yang Song
University of Wisconsin-Milwaukee

Follow this and additional works at: https://dc.uwm.edu/etd

Part of the Geography Commons

EXAMINING URBAN HEAT ISLAND EFFECT AND ITS PUBLIC HEALTH IMPLICATIONS WITH REMOTELY SENSED DATA

by

Yang Song

A Dissertation Submitted in

Partial Fulfilment of the

Requirements for the Degree of

Doctor of Philosophy

in Geography

at

The University of Wisconsin-Milwaukee

May 2018

ABSTRACT
EXAMINING URBAN HEAT ISLAND EFFECT AND ITS PUBLIC HEALTH IMPLICATIONS WITH REMOTELY SENSED DATA

by
Yang Song
The University of Wisconsin-Milwaukee, 2018
Under the Supervision of Professor Changshan Wu

The Urban heat island (UHI) as a byproduct of urbanization has long been studied utilizing remote sensing technologies. However, issues remain to be addressed. Land surface temperature (LST) as the indicator of surface UHI can be retrieved from remotely sensed data, but its accuracy is limited as existing studies neglect the neighboring effect. Further, while LST serves well as an indicator of surface thermal condition, it lacks the ability to reveal human heat stress, which is an environmental hazard that can seriously affect productivity, health or even survival of individuals. Although human heat stress has long been studied and can be quantified by many heat stress indices, it has never been explored across continuous spaces. Aiming to address these issues, the objectives of this research include: (1) taking into account the neighboring effect during LST retrieval using a moving window method; (2) revealing human heat stress with remotely sensed data; and (3) exploring the relationship between heat stress and land cover composition and configuration. My results indicate that the accuracy of LST estimation is improved when neighboring effect is considered. Discomfort index (DI) as an indicator of human heat stress can be retrieved from remotely sensed data, and its spatial distribution and relationship with land cover composition is largely affected by relative humidity. Spatial configuration of different land covers has an impact on DI, which may provide insights for policy makers and urban designers on mitigating hazardous environmental effect brought by urbanization.

TABLE OF CONTENTS

LIST OF FIGURES

LIST OF TABLES

CHAPTER 1 INTRODUCTION

1.1 Background

The world has experienced high intensity urbanization since the second industrial revolution. Indeed, the ratio of people who reside in urban areas increased from 13.3% to 29.4% during the first half of 20th century, and is projected to reach 67% in 2050 (United Nations, 2012). With the rapid expansion of cities around the world, plenty of natural and rural land uses such as forest, grassland and agriculture have been converted to urban areas covered by buildings, roads and pavements etc. Modifications of the earth surface and atmosphere brought by urbanization usually leads to a climate warmer than the surrounding rural areas (Voogt and Oke, 2003). This phenomenon is defined as the urban heat island (UHI).

As a widely existing phenomenon, UHI originates from the distinct thermal energy transmission processes in rural and urban areas. Thermal energy generated and contained in an area has two main sources: solar radiation from the sun and anthropogenic heat from power plants, automobiles and air conditioners etc. (Avissar, 1996). In rural areas (generally covered by vegetation and soil), solar radiation is the dominant source and anthropogenic heat is generally negligible. As solar radiation arrives at ground surface, part of it is absorbed and converted into thermal energy which is mostly consumed and returned to atmosphere due to evapotranspiration. Thus, thermal energy in rural areas is usually in a dynamic balance which leads to a stable and lower temperature. In urban areas, however, evapotranspiration barely exists due to the lack of vegetation. Solar radiation captured by the ground surface is converted into thermal energy and stored in artificial materials such as asphalt, cement and plastic, etc. Meanwhile, large amount of

1

heat generated from human-related behaviors in urban areas intensifies the thermal energy stored in urban areas. As a result, urban areas usually have higher temperatures, which makes them warmer islands surrounded by cooler rural areas.

Traditional ground-based observations carried out by thermometer networks or by thermometers mounted on vehicles have long been utilized to study the UHI. As the basis of UHI research, numerical models were developed to quantitatively describe the energy balance in urban areas. Myrup (1969) described a numerical energy budget model and applied it to the urban atmosphere. It successfully predicted the magnitude of urban temperature excesses. Oke and Nunez (1980) systematically analyzed the energy balances in both rural and urban areas. They divided the urban vertical profile into canopy layer and boundary layer, and built energy models separately for them. Subsequently, studies have explored mitigation of the adverse thermal effects of UHI. Oliveira et al. (2011) analyzed the thermal performance of a small park in Lisbon, and concluded that even green areas with small sizes have the potential of mitigating the UHI. Alexandri and Jones (2008) developed a two-dimensional urban canyon model, and simulated the cooling effect brought by green walls and roofs with climatological data acquired from nine cities around the world with different climates. Ca et al. (1998) studied the UHI mitigation effect of a park from the perspective of energy saving. Their research confirmed the presence of a park can improve the thermal environment of urban areas, and 4000kW/h of electricity for cooling can be saved within 1 hour of a hot summer day. In addition, given the adverse influence of high temperature on human health, the relationship between UHI and human heat stress has also drawn attention from researchers. Steeneveld et al. (2011) quantified human comfort with approximate wet bulb globe temperatures (AWBGT) in 27 Dutch cities.

Results indicated that nearly 50% of the cities in the study are subject to heat stress about 7 days a year. Heusinkveld et al. (2010) employed a physiological equivalent temperature to indicate human heat stress and evaluate the intensity of UHI. The research revealed that green areas in the city are helpful in alleviating heat stress brought by UHI. Other human comfort indicators have also been proposed in earlier studies such as a cooling power index (Balaras et al., 1993), the particular vote (Hoppe, 2002) and discomfort index (Kolokotsa et al., 2009). However, many of these indices are barely utilized in studies of UHI, due to the requirement of human metabolic information.

With the advent of remote sensing technology, large scale and multi-temporal observation of UHI become possible utilizing land surface data acquired by satellite and airborne platforms. Remote sensors observe the UHI by detecting the upwelling thermal radiance from the earth's surface (Voogt and Oke 2003). In other words, land surface temperature (LST) is the main indicator of UHI when remote sensing technology is employed. Trying to connect LST to air temperature, many efforts have been made to find the numerical relationship between them (Prihodko and Goward, 1997; Cresswell et al., 1999; Cristobal et al., 2008; Vancutsem et al., 2010). However, only empirical models based on the local data were built due to the complexity of the energy transmission in the lowest atmospheric layers. An effective model connecting LST and air temperature has not yet been built. Meanwhile, remote sensing indices and land cover characteristics retrieved from remote sensing images have been employed to describe UHI by exploring their relationship with LST (Carson et al., 1994; Lo et al., 1997; Weng, 2001; Weng et al., 2004; Yuan and Bauer, 2007). The commonly used indicators of LST include normalized difference vegetation index (NDVI), normalized difference built-up index (NDBI), vegetation

3

fraction (%GV) and impervious surface fraction (%ISA). Although their performance may vary due to different study areas, research scale or even the method employed to retrieve them, they do provide different perspectives to study UHI with remote sensing technologies.

Even though UHI has long been studied with both traditional meteorological and remotely sensed data, there are two challenging problems. First, the study of UHI with remote sensing imagery focuses on analyses of single pixels, which may neglect the potential influence of neighboring environments in the research of UHI. Further, although LST has long been the main indicator of surface thermal condition when remotely sensed data are employed, it may fail to address human heat stress afflicted by hot environment, as associated factors such as air temperature and relative humidity, cannot be explained by LST.

1.2 Problem statement

Neighboring effect refers to the characteristics of an area being not only decided by itself, but also affected by its surroundings. Specifically, LST of an area is not only related to each location's thermal condition and land cover composition, but also affected by its surrounding environment. For example, a freeway made of asphalt goes through a city which includes downtown, residential areas, suburbs, and then leaves the city along a lake shore. Although the road is all covered with asphalt, LST of the road may differ dramatically from one segment to another due to the distinct surrounding environments. Current studies of UHI with remotely sensed data usually utilize either radiative information acquired by thermal sensors or remote sensing indicators and land cover fractions to estimate LST (Schmugge et al., 1998; Qin et al.,

4

2001; Gallo, 1993; Lo et al., 1997; Gallo and Owen, 1999). However, most studies are carried out by treating each pixel as a standalone object and neglect the possible interactions among neighboring pixels which could affect the value of LST. The lack of neighboring information may lead to a biased evaluation of the relationship between these indicators and LST. Therefore, a method that considers the neighboring effect is needed for the quantitative analysis of LST.

A crucial requirement for normal human body function is that body temperature needs to stay in a narrow range of $\pm1^{o}C$ around the resting body core temperature of $37^{o}C$ (Epstein and Moran, 2006). Exposure to high temperature environments may cause heat stress and therefore affect work efficiency, productivity and even threaten survival (Epstein et al., 1980; Bell, 1981). As the main sites of human habitation, urban areas also increase heat stress due to the UHI. Assessment of heat stress has drawn much attention from physiology and public health sciences for over a century (Epstein and Moran, 2006). Integrating environmental and physiological variables, many indices have been suggested to satisfactorily describe heat stress (Haldane, 1905; Dufton, 1929; Belding and Hatch, 1955; Gonzales et al., 1978; Frank et al., 1996; Wallace et al., 2005). In urban areas, environmental variables such as air/surface temperature, wind velocity and humidity may change from one site to another, which leads to a spatially uneven distribution of heat stress across the city. Heat stress indices which were constructed based on the data from a single station or average values fail to address this issue. Spatial information has barely been taken into account when heat stress is assessed. Thus, investigation of heat stress in urban areas from a spatial perspective becomes an important research challenge.

In summary, the objectives of this proposed research include: (1) addressing the neighboring effect in the quantitative analysis of UHI; (2) revealing human heat stress in continuous space at mesoscales with remotely sensed data; and (3) exploring the connection between human heat stress and land cover spatial composition and configuration.

1.3 Literature review

1.3.1 Revealing UHI with remotely sensed data

Since LST is a main indicator of UHI when remotely sensed data are employed, the accurate estimation of LST becomes the cornerstone of any research on UHI with remote sensing technology. Methods developed for the estimation of LST with remotely sensed data can be categorized into two groups. The first group utilizes radiative information collected by thermal sensors, or specifically, top of atmosphere (TOA) radiance (or at-sensor radiance) to retrieve LST. Meanwhile, the second group explores the statistical relationship between LST and remote sensing indices or land cover fractions, and predicts LST based on statistical models.

Radiative transfer equation (RTE) is a representative of the first group (Palluconi and Meeks, 1985). It quantitatively describes the radiative transmission process rationale in the atmosphere and links TOA radiance, land surface emissivity, and downwelling/upwelling atmospheric radiance to LST with a single equation. Schmugge et al. (1998) employed RTE to retrieve LST from thermal infrared multiple scanner (TIMS) images acquired in Africa. Results indicated that image-retrieved LST were in good agreement with ground-based measurements. In order to avoid the dependence on complex atmosphere radioactive conditions in the RTE approach, Qin

6

et al. (2001) proposed a mono-window algorithm for LST retrieval with Landsat Thematic Mapper (TM) band 6 data. It avoids the use of downwelling/upwelling atmospheric radiance by utilizing mean atmospheric temperature in the calculation of LST, and provides an accurate estimation of LST from TM data. Jemenez and Sobrino (2003) have also developed a generalized single-channel method to retrieve LST from a single thermal channel. In this method, three functions of total atmospheric water vapor content were obtained from a simulation, and utilized to retrieve LST with TOA radiance. This method can be applied to any thermal sensor and provided a new perspective of LST retrieval by utilizing atmospheric water vapor content in the calculation.

Except single-channel methods which utilize the information from one infrared channel to determine LST, split window techniques use differential absorption of two channels within one atmospheric window to eliminate the atmospheric influence, and calculate LST as a linear combination of two brightness temperatures (Price, 1984; Becker and Li, 1990; Sobrino et al., 1991). Although split window methods are computationally simple, they are difficult to apply at a global scale since parameters are valid only for a specific area (Dash et al. 2002). In summary, group one methods are developed based on the radiative transfer theory and have solid physical bases. With the support of sufficient atmospheric radiative parameters, they provide very accurate estimation of LST. Therefore, LST retrieved from group one methods are usually employed as "true values" of a specific area instudies of UHI with remotely sensed data. However, drawbacks of group one methods are also evident: they are computationally complex and depend too much on the accuracy of atmospheric parameters that are usually difficult to acquire.

In order to avoid the complexity of the first group methods, remote sensing indices and land cover fractions were employed to predict LST based on empirical models. In earlier remote sensing studies on UHI, NDVI was the major indicator of urban climate due to its negative correlation with air and surface temperature. Gallo et al. (1993) retrieved NDVI and LST of 37 US cities and nearby rural areas from AVHRR data, and assessed the influence of urban environments on observed minimum air temperature. They found that NDVI explained a great amount of the minimum temperature differences between urban and rural areas. Lo et al. (1997) used NDVI retrieved from the Advanced Thermal and land Applications Sensor (ATLAS) to study changes of thermal responses of urban land covers between day and night, and examined the relationship between land cover irradiance and vegetation amount. The study concluded that vegetation associated land cover types, such as residential and agricultural, play a vital role in lowering LST of urban areas. In contrast, Weng et al. (2004) argued that NDVI is insufficient to estimate LST since NDVI has a nonlinear relationship with vegetation abundance (Asrar et al., 1984) and depends too much on specific remote sensing platforms (Small, 2001). They therefore proposed an approach which utilizes vegetation fraction (%GV) of each pixel to estimate LST. Results indicated that %GV has a slightly stronger negative correlation with LST than NDVI at all examined spatial resolutions (30 to 960m), with the correlation reaching its peak at 120m resolution. Yuan and Bauer (2007) also pointed out NDVI is not sufficient for LST estimation due to its nonlinear correlation with LST and seasonal variability. Given the positive correlation between %ISA and LST, they found an extremely strong linear relationship between mean LST and %ISA.

1.3.2 Human heat stress indices

Heat stress is a common concern for humans, especially for people with specific occupations such as soldiers, athletes and construction workers. It can severely influence the productivity and health of an individual (Epstein and Moran, 2006). In order to relate physiological heat strain perceived by an individual to the heat stress one is exposed to, many studies have focused on estimating the stress originating from work environments or climate through a single heat stress index (Haldane, 1905; Hill et al., 1916; Dufton, 1929; Belding and Hatch, 1955; McKarns and Brief, 1966; Gonzales et al., 1978; Frank et al., 1996; Wallace et al., 2005). Heat stress indices proposed so far can be categorized into three groups: rationale indices, empirical indices and direct indices (Epstein and Moran, 2006). Calculation of the first two groups is usually complicated and requires both environmental and physiological data, which is beyond the scope of this research. The direct indices, however, are based on measurement of basic environment variables, and thus have the potential to be implementedusing remotely sensed data.

Houghton and Yaglou (1923) proposed effective temperature (ET), which is considered the first direct heat stress index. It was established to provide a measurement of temperature and humidity on human comfort. In order to take the influence of thermal radiation into account, Vernon and Warner (1932) utilized black-globe temperature to modify ET, and established corrected effective temperature (CET). Since then, CET has been respected as a basic index to which many modifications were made. As the most widely utilized heat stress index, wet-bulb globe temperature (WBGT) was developed by the US Navy as a part of a study associated with heat related injuries during military training (Yaglou and Minard 1957). The WBGT index is easy to calculate as a linear combination of weighted dry-bulb temperature, wet-bulb temperature

9

and black-globe temperature. Coefficients in WBGT were determined empirically and no physiological variables are needed to calculate the index. In spite of the simplicity of WBGT, its limitation lies in the applicability across a broad range of environments, due to the inconvenience of of black-bulb temperature measurements. The Oxford index (WD) was subsequently proposed by Lind and Hellon (1957) to avoid using black-bulb temperature when thermal radiation can be neglected. Effectiveness of WD was demonstrated by the high correlation with physiological tolerance time, which is the time to reach a rectal temperature of 39.2 ^{o}C and/or heart rate of 180 bmp. Although WD was argued as not appropriate when there is significant thermal radiation, many other indices were proposed based on it due to its ease of calculation (Thom, 1959; Moran et al., 1998; Moran et al., 2001).

Many heat stress indices have been developed and long utilized to evaluate the thermal condition for limited scenarios such as military training fields, construction sites or industrial facilities. However, as urban areas rapidly spread around the world, heat stress associated with UHI is becoming a threat to the health of common citizens. An easily used index which is able to reveal the distribution of heat stress across the whole city instead of specific interest sites will help urban planners and policy makers better address the issue and therefore lead to a better solutions to the challenges of UHI.

CHAPTER 2 EXAMINING THE IMPACT OF URBAN BIOPHYSICAL COMPOSITION AND NEIGHBORING ENVIRONMENT ON SURFACE URBAN HEAT ISLAND EFFECT

2.1 Introduction

Urban heat island (UHI) refers to the phenomenon that apparent higher temperatures are found in urban areas when compared to surrounding rural areas, primarily due to atmospheric and surface modifications associated with urbanization (Voogt and Oke, 2003). Concentrated human activities in urban areas have led to abundant energy emissions, affecting regional climate by altering energy exchange and heat conductivity (Yuan and Bauer, 2007). Voogt and Oke (2003) divided the UHI into three categories: canopy layer heat island (CLHI), boundary layer heat island (BLHI) and surface urban heat island (SUHI). The first two categories can be identified as an atmospheric heat island, which is usually described using air temperature records collected by in-situ measurement and records from weather stations, while SUHIs are often characterized by land surface temperature (LST) retrieved from airborne and satellite remote sensing imagery.

In the study of SUHI, remote sensing technology has played an important role due to its ability to extract information for large geographical areas with repetitive coverage. When SUHI is studied using remotely sensed data, the normalized difference vegetation index (NDVI) has been employed as the main indicator of LST. As it indicates abundance of green vegetation, a higher

NDVI value usually means a lower LST value due to evapotranspiration. The relationship between NDVI and LST has been applied to many SUHI related studies. Gallo et al. (1993) analyzed the urban-rural difference of NDVI and LST, and evaluated the impact of urban areas on minimum air temperature. Gallo and Owen (1999) reported that 40% of urban-rural temperature differences can be explained by differences in NDVI and satellite image derived LST. Lo et al. (1997) analyzed the differences of thermal response of different land cover types between day and night, and investigated the relationship between surface radiance and NDVI.

With the development of spectral mixture analysis, land cover fractions were then employed to retrieve LST from remote sensing imagery. Weng et al. (2004) utilized vegetation fraction (%GV) as an indicator of LST in the City of Indianapolis, Indiana (United States). Results demonstrated that LST has a slightly stronger correlation with %GV than NDVI at all selected scales (30m, 60m, 120m, 240m, 480m and 960m). Yuan and Bauer (2007) calculated mean values of LST for each 1% increment of NDVI and impervious surface fraction (%ISA) for a TM image of Twin Cities, Minnesota (United States). The result indicated that %ISA has abetter linear relationship with mean LST than NDVI during all four seasons. Li et al. (2011) also found a strong relationship between %ISA and mean LST when investigating the influence of landscape structure on UHI in Shanghai, China. Despite the better performance of land cover fractions in recent studies, several issues still exist. First, when %GV is employed as the single indicator of LST, all pixels occupied by non-vegetation land covers have similar values of %GV and are considered to have similar thermal characteristics. However, LST could be unstable even for the same land cover type. Taking soil cover for instance, LST could differ dramatically as the humidity of soil cover changes, even with the same %GV. In other words, different land covers

should be discriminated and discussed separately during the process of LST estimation, especially for areas not dominated by vegetation. Second, when %ISA is applied to study SUHI, the relationship between the mean values of LST and %ISA was examined (Yuan and Bauer, 2007). Urban impervious surfaces, however, represent a collection of materials water cannot infiltrate, and may include a number of specific materials with different thermal characteristics. Mean values of LST may bring a strong statistical relationship with %ISA, but the thermal differences among various impervious surfaces may be neglected. Therefore, it is arguable whether %ISA is a reasonable indicator of LST in urban areas.

In addition to the influence from different land cover types, another key factor that could affect LST in urban areas is the surrounding environment. For instance, a highway made of asphalt goes through a city which includes downtown, residential areas and suburbs. Although the road is made of single material, LST may differ dramatically from one segment to another due to the distinct surrounding environment. In downtown, road LST is usually higher due to the massive anthropogenic heat emitted by air conditioning systems and vehicles. Meanwhile, above road temperature may decrease due to the surrounding forests in suburban areas. Therefore, in order to accurately estimate LST in urban areas, the influences of surrounding environments should be considered. Currently, however, SUHI studies with remote sensing imagery are carried out by treating each pixel as a standalone object and ignore the possible influences from neighboring pixels which could affect LST. The lack of neighboring information may lead to a biased estimation of LST. A method considering the neighboring effect is urgently needed for improved quantitative estimation of LST.

In order to address the aforementioned issues, the performance of spectral indices (NDVI and NDBI) and landcover fractions (%GV and %ISA) as indicators of LST were examined first in our study. Then, we analyzed large LST variations in non-vegetated areas and related them to the influence of surrounding environments on the LST of impervious surfaces. Lastly, a method considering the neighboring effect was proposed to incorporate the influence from surrounding environments into the estimation of LST.

2.2 Study area and data

Four counties (Milwaukee, Waukesha, Washington and Ozaukee), located in Wisconsin (United States) were selected as the study area (Figure 1). These four counties cover a geographic area of 3,784 km^2 with a population of 1.6 million (U.S. Census Bureau, 2010). The average population and household numbers have increased by 3.5% and 7.0% annually since 1980 (Southeastern Wisconsin Regional Planning Commission [SEWRPC], 2010; U.S. Census Bureau, 2010). Moreover, according to the analyses based on historical socio-economic data, this trend will continue over the next several decades (SEWRPC, 2004a, 2004b). There are various land use/land cover types within the study area, including industrial, transportation, residential, commercial, agricultural, water bodies and open lands such as forest, wetland and barren land (SEWRPC, 2000). As the major urbanized area of Wisconsin, the City of Milwaukee has more than 60% of the total population of the study area.

In order to examine the SUHI effect within the study area, several requirements must be satisfied, including: 1) the availability of high spatial resolution imagery; 2) the need forthermal

14

imagery to allow for LST retrieval; 3) as little cloud cover over the study area as possible; and 4)

multiple images for time series analysis. Thus, a Landsat ETM+ image and two TM images

acquired on July 9th, 2001, July 15th, 2006 and June 24th, 2010, respectively, were obtained

from the U.S. Geological Survey (USGS). TM images were employed since Scan Line Corrector

(SLC) of Landsat 7 ETM+ stopped working after May 31, 2003. As the first seven bands of

ETM+ and TM have the same spatial and spectral configuration (except the spatial resolution of

the thermal band [band 6]), TM images were obtained to replace ETM+ data for year 2006 and

2010. All images were rectified to a Universal Transverse Mercator (UTM) projection with the

WGS84 coordinate system by USGS. Optical bands, including visible, near-infrared (band 1-4)

and shortwave infrared (band 5 and 7) bands were employed for deriving fraction land covers

and calculating spectral indices. Band 6 was utilized to retrieve land surface temperature (LST).

It is noteworthy that although the original spatial resolution of ETM+ and TM thermal band is 60

meters and 120 meters respectively, images released by USGS had been resampled to 30 meters.
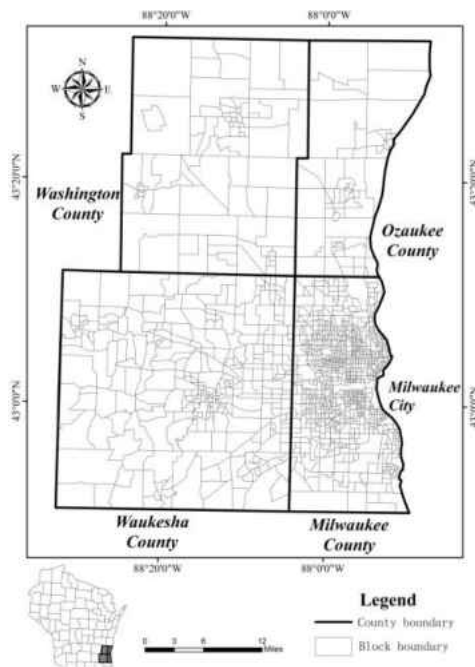
Figure 1 Study area (Milwaukee and three adjacent counties)

15

2.3 Methods

2.3.1 LST retrieval

The mono window algorithm (MWA) (Qin et al., 2001) was employed to retrieve LST. MWA

utilizes remotely sensed thermal data and meteorological data to obtain LST, and the following

equation is applied to calculate LST values.

$$T_s = [a_6(1 - C_6 - D_6) + (b_6(1 - C_6 - D_6) + C_6 + D_6)T_6 - D_6 T_a]/C_6 \qquad (1)$$

with

$$C_6 = \varepsilon_6 \tau_6 \qquad\qquad (2)$$

$$D_6 = (1 - \tau_6)[1 + (1 - \varepsilon_6)\tau_6] \qquad\qquad (3)$$

where T_a is the effective mean atmospheric temperature; T_6 is the brightness temperature of

ETM+ thermal band 6; τ_6 is the atmospheric transmittance of ETM+ band 6 on the date when

this image was acquired; ε_6 is the emissivity of ETM+ band 6; $a_6 = -67.355351$ and $b_6 =$

0.458606 are constants. In order to retrieve LST, T_a, T_6, τ_6 and ε_6 are yet to be determined.

Determination of effective mean atmospheric temperature (T_a)

Since the study area is located in the mid-latitude region and the ETM+ image was acquired in

summer, a regression model proposed by Qin et al. (2001) for summer mid-latitude regions was

employed to determine effective mean atmospheric temperature (Equation 6).

$$T_a = 0.92621 T_0 + 16.011 \qquad\qquad (4)$$

where T_0 in Kelvin (K) is near-surface air temperature acquired by field measurement.

Determination of brightness temperature (T_6) and atmospheric transmittance (τ_6)

At-satellite brightness temperature of ETM+ images can be retrieved using the equations in

Markham and Barker's work (1986) and Landsat 7 science data user's handbook (Irish, 2000).

$$T_6 = \frac{K_2}{\ln\left(\frac{K_1}{L_\lambda}+1\right)} \hspace{4cm} (5)$$

with

$$L_\lambda = \frac{L_{max}-L_{min}}{QCAL_{max}-QCAL_{min}}(DN - QCAL_{min}) + L_{min} \hspace{1.5cm} (6)$$

where T_6 is at-satellite brightness in Kelvin; L_λ is the radiance at wavelength λ received by ETM+

sensor; $QCAL_{max}$ (=255) and $QCAL_{min}$ (=1) are the maximum and minimum values of DN

respectively. L_{max} and L_{min} are top-of-atmospheric (TOA) radiances scaled to $QCAL_{min}$ and

$QCAL_{max}$.

Atmospheric transmittance (τ_6) was acquired by utilizing an atmospheric correction tool

developed by Barsi et al. (2005). This tool is available at NASA's website

(http://atmcorr.gsfc.nasa.gov) and uses the MODTRAN radiative transfer model and a suite of

algorithms to estimate atmospheric transmittance, upwelling radiance and downwelling radiance.

Determination of emissivity (ε_6)

The NDVI threshold method was employed to determine the emissivity of different land cover types (Sobrino et al, 2000). This method divides all pixels into three groups (fully vegetated, partly vegetated and non-vegetated) according to NDVI values and calculates emissivity respectively. Comparing to algorithms based on Temperature-Independent Spectral Indices (TISI), the NDVI threshold method is not dependent on short-wave infrared band information and thus compatible with all data as long as NDVI can be retrieved (Sobrino et al, 2001). First, water pixels were obtained using iterative self-organizing data analysis (ISODATA) (Tou & Gonzalez, 1974), and assigned 0.99 as emissivity (Okwen et al., 2011). Pixels with NDVI larger than 0.5 were considered fully vegetated and assigned 0.985. Then non-water pixels with NDVI less than 0.2 were considered as non-vegetated and given a value of 0.972 (Snyder et al., 1998; Sobrino, 2001). Finally, pixels with NDVI between 0.2 and 0.5 were considered as mixed ones which were covered by various land cover types, such as vegetation, impervious surfaces and bare soil. The following equations (Carlson & Ripley, 1997; Sobrino, 2001) were utilized to calculate the emissivity of mixed pixels.

$$\varepsilon_{mix} = \varepsilon_v p_v + \varepsilon_n (1 - p_v) + C_i \tag{7}$$

with

$$p_v = \left(\frac{NDVI - NDVI_{min}}{NDVI_{max} - NDVI_{min}}\right)^2 \tag{8}$$

$$C_i = (1 - \varepsilon_n)(1 - p_v)F\varepsilon_v \tag{9}$$

where ε_{mix} is the emissivity of mixed pixels; ε_v (=0.985) and ε_n (=0.972) are emissivity of fully vegetated and non-vegetated pixels, respectively; $NDVI_{max}$ and $NDVI_{min}$ are maximum and minimum NDVI values among all non-water pixels, respectively; p_v is the scaled NDVI value; $F = 0.55$ is factor related to geometrical distribution (Sobrino et al., 1990).

2.3.2 Normalization of LST

As three images acquired from different years were employed in this study, it is difficult to conduct a comparative analysis as the range of LST differs from one image to another. Therefore, LST was scaled between minimum and maximum values. These values were firstly identified in each LST image, and then utilized to normalize LST (Amiri et al., 2009):

$$T'_s = \frac{T_s - T_{min}}{T_{max} - T_{min}} \tag{10}$$

where T_s is the LST for a given pixel; T_{max} and T_{min} are the maximum and minimum LST within an image, respectively; T'_s is the normalized LST.

2.3.3 Calculation of NDVI, NDBI and BCI

In order to evaluate the performance of vegetation and impervious surface fractions as indicators of LST, normalized difference vegetation index (NDVI) and normalized difference building index (NDBI) were employed for comparison. NDVI is a spectral index which addresses vegetation abundance by normalizing the difference of vegetation reflectance in near infrared and red bands. Similarly, NDBI is a spectral index to map built-up areas using reflectance of near-infrared and shortwave infrared bands (Zha et al., 2003). NDBI can be considered as an indirect indicator of impervious surfaces and is expected to be positively correlated with impervious surfaces abundance.

$$NDVI = \frac{NIR - RED}{NIR + RED} \tag{11}$$

$$NDBI = \frac{SWIR - NIR}{SWIR + NIR} \tag{12}$$

where NIR, RED and $SWIR$ are the reflectances of near-infrared, red and shortwave infrared bands respectively.

The biophysical composition index (BCI) (Deng & Wu, 2012) was also employed to distinguish impervious surfaces from soil in the image. Calculation of BCI is based on the result of tasseled cap (TC) transformations, which were originally proposed to identify agricultural crops (Kauth and Thomas, 1976). However, Deng and Wu (2012) utilized it to identify typical urban biophysical compositions by normalizing the first three TC components:

$$H = \frac{TC1 - TC1_{min}}{TC1_{max} - TC1_{min}} \qquad (13)$$

$$V = \frac{TC2 - TC2_{min}}{TC2_{max} - TC2_{min}} \qquad (14)$$

$$L = \frac{TC3 - TC3_{min}}{TC3_{max} - TC3_{min}} \qquad (15)$$

where H is high albedo materials addressed by normalized $TC1$; L is low albedo materials addressed by normalized $TC2$; V is vegetation addressed by normalized $TC3$. TCi (i=1,2,3) are the first three components of TC transformation; TCi_{max} and TCi_{min} are the maximum and minimum values of the ith TC component; Then BCI can be given by the following equation:

$$BCI = \frac{(H+L)/2 - V}{(H+L)/2 + V} \qquad (16)$$

2.3.4 Retrieval of land cover fractions

Following, Ridd's (1995) V-I-S model, land cover fraction of vegetation (%GV), impervious surface (%ISA) and soil (%Soil) will be retrieved utilizing constrained linear mixture analysis

(LSMA). LSMA assumes that the spectrum of each pixel is a linear combination of the spectra of all homogeneous landcover types (endmembers) within the pixel (Adams et al., 1995; Roberts et al., 1998). The mathematical model of LSMA can be expressed as:

$$R_b = \sum_{i=1}^{N} f_i R_{i,b} + e_b \tag{17}$$

subject to

$$\sum_{i=1}^{N} f_i = 1, f_i \geq 0 \tag{18}$$

where R_b is the reflectance of band b; N is the number of endmembers selected from the image; f_i is the fraction of endmember i; $R_{i,b}$ is the reflectance of endmember i at band b; and e_b is model residual.

Prior to LSMA, a minimum noise fraction (MNF) transformation was applied to reduce correlations among optical bands (band 1-5, 7) and data redundancy (Wu & Murray, 2003). Four endmembers (high albedo material, low albedo material, vegetation and soil, Figure 2) were initially selected according to the feature space scatterplots of the first three MNF components (Figure 3). Then these initial endmembers were visually verified through comparison with high-resolution aerial photographs. Ridd's (1995) V-I-S conceptual model was employed to describe the land cover composition for the study area. Thus, %ISA is considered as the sum of high and low albedo material fractions following the work of Wu and Murray (2003).
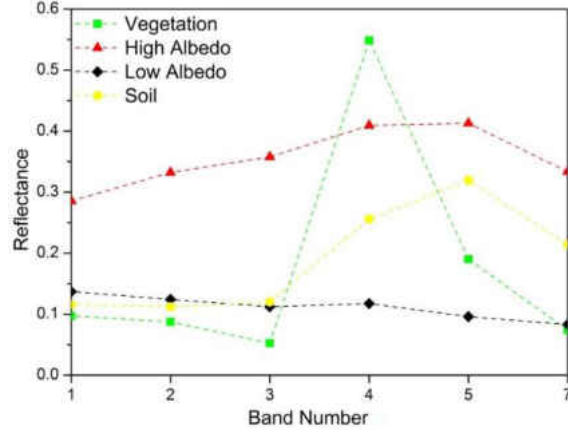
Figure 2 Average reflectance spectra of endmembers
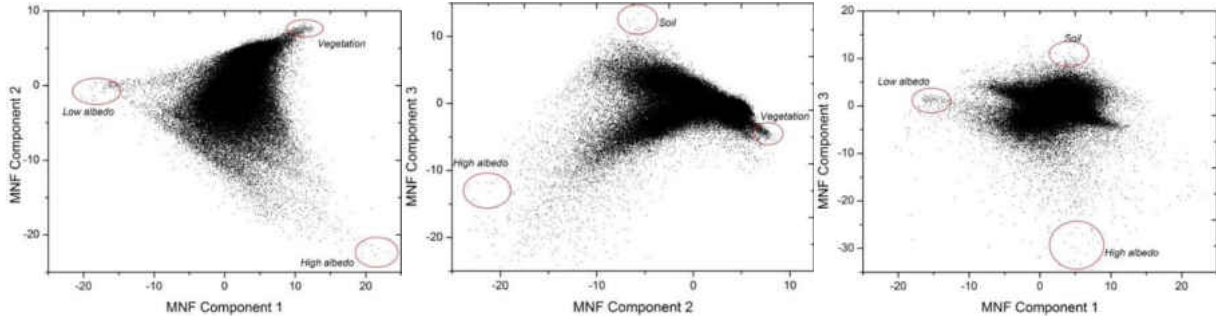
Figure 3 Endmember selection in the feature space of MNF transformation

The accuracy of SMA retrieved land cover fractions were assessed using 1-meter digital aerial ortho-imagery acquired from springs of year 2000, 2006 and 2010. Root mean square error (RMSE) and mean absolute error (MAE) were employed as metrics for accuracy assessment of land cover fractions of each image. They can be expressed as follows:

$$\text{RMSE} = \sqrt{\frac{1}{N}\sum_{1}^{N}(LF_i - LF_i')^2} \qquad (19)$$

$$\text{MAE} = \frac{1}{N}|LF_i - LF_i'| \qquad (20)$$

where LF_i is SMA retrieved land cover fraction for pixel i; LF_i' is the actual land cover fraction calculated from digital aerial orthoimagery for pixel i. N is the total number of pixels employed

22

for accuracy assessment and equals 100 in my study. RMSE and MAE are both metrics of precision which quantify the relative error of land cover fractions retrieved by SMA at pixel level (Table 1).

Table 1 Accuracy assessment of land cover fractions

	RMSE			MAE		
	2001	2006	2010	2001	2006	2010
%GV	0.049	0.060	0.050	0.036	0.042	0.037
%ISA	0.770	0.064	0.091	0.041	0.042	0.046
%Soil	0.111	0.110	0.112	0.093	0.095	0.101

2.3.5 Addressing the impact of neighboring environment on LST

Two indicators are proposed to quantify the neighboring effect as follows:

$$\overline{LST}_d = \frac{\sum_i^n (LST_c - LST_i)}{n} \tag{21}$$

$$\overline{NDVI}_d = \frac{\sum_i^n (NDVI_c - NDVI_i)}{n} \tag{22}$$

where LST_c and $NDVI_c$ are the LST and NDVI of the central pixel within a 3x3 pixel window; n is the total number of neighboring pixels and equals 8 for the 3x3 pixel window employed in the research; i is the number of each neighboring pixel within the window;. $\overline{LST}_d$ represents the average difference in LST between each pixel and its neighboring pixels. Larger $\overline{LST}_d$ means higher LST gradient between a pixel and its surroundings, and indicates stronger SUHI intensity around this pixel. $\overline{NDVI}_d$ indicates the average difference in vegetation abundance between each pixel and its neighboring pixels. It is utilized to relate SUHI intensity to the cooling effect of vegetation.

In order to address the influence of the neighboring environment on LST, an average filter method was employed. By creating a window with a specific size (e.g. 3x3 or 5x5 pixel) on the image, the average %ISA within the moving window was calculated and given to the central pixel. As the window moves across the image, %ISA of every pixel in the image is recalculated. In this study, five window sizes (e.g. 3x3, 5x5, 7x7, 9x9, and 11x11 pixel) were applied and the original image was considered the result of an average filter with a 1x1 pixel window. Then linear regression between recalculated %ISA and LST was performed based on each window size.

2.4 Results

2.4.1 Spatial distribution of SUHI

LST retrieved from the remotely sensed data can be utilized to reveal the spatial distribution of SUHI (Figure 4). The retrieved LST varies in different ranges among the different years, yet high values are located in the central business district of the city of Milwaukee during all three years. A clear SUHI effect can be observed from Fig. 4 with dramatic urban-rural temperature contrasts. The Milwaukee metropolitan area is the highpoint of LST within the study area. Several hot spots can also be identified in the north and northwest portions of the city of Milwaukee. Roads radiating from downtown Milwaukee have higher LST than their surroundings (they appear as bright lines in the images. There are also clear linear pattern along the highways to the north and west of Milwaukee.
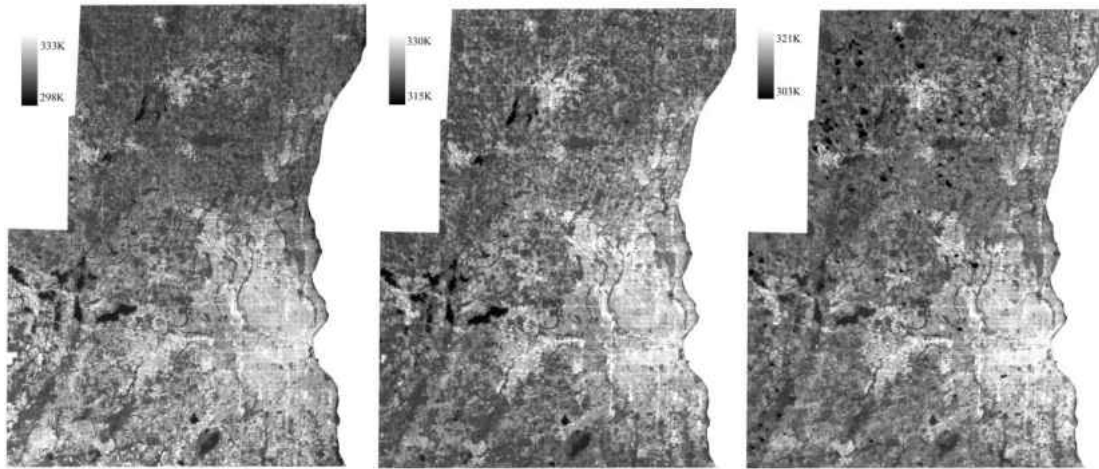
Figure 4 LST of the study area

2.4.2 Comparative analysis of spectral indices and land cover fractions as LST indicators

NDVI and %GV

NDVI maps for the study area are shown in Figure 5. Although the min and max values of NDVI varies in different images, more than half of each image are covered by bright pixels, which can be identified as fully vegetated. Urban areas, with low or negative NDVI values, are mainly found in Milwaukee County and the eastern parts of Waukesha County. Vegetation fraction maps indicates the same spatial pattern of vegetation distribution.

In order to compare the performance of spectral indices and land cover fractions as LST indicators, ten thousand non-water pixels were randomly selected across the study area for linear regression. Scatter plots of NDVI, %GV and LST are shown in Figure 7. Results indicate that NDVI has a better linear relationship with LST comparing to %GV. Further, linear correlation

25

between NDVI and LST becomes weak when NDVI decreases. This indicates that LST varies

dramatically in non-vegetated areas covered by impervious surfaces and soil.

| (a) NDVI 2001 | (b) NDVI 2006 | (c) NDVI 2010 |

| (d) %GV 2001 | (e) %GV 2006 | (f) %GV 2010 |
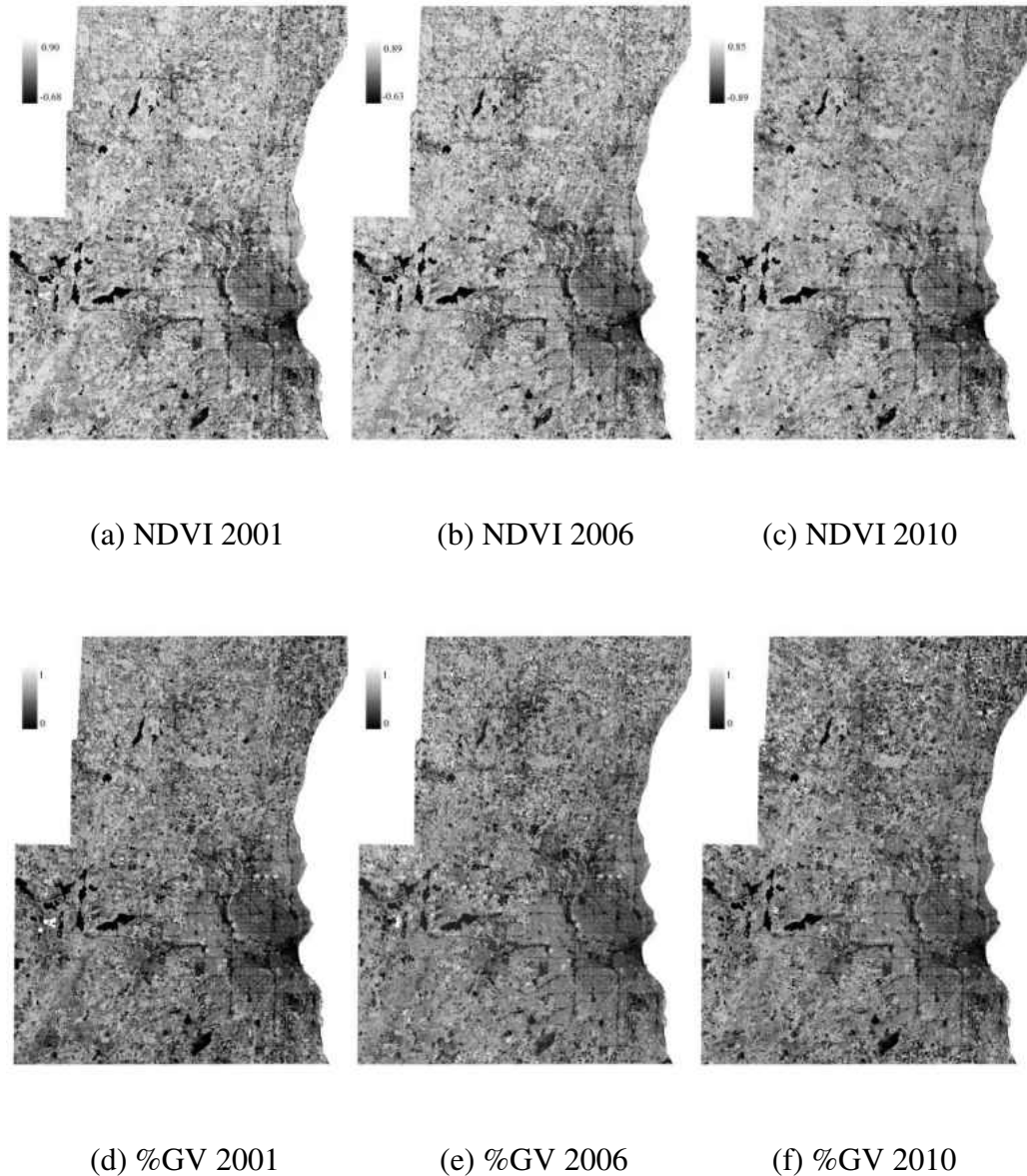
Figure 5 NDVI (a, b and c) and %GV (d, e and f) of the study area

NDBI and %ISA

Since NDBI and %ISA both indicate the abundance of impervious surfaces (Figure 6), they are

mutually exclusive with NDVI and %GV. However, similar to the comparison between NDVI

26

and %GV, NDBI has stronger linear correlations with LST than %ISA does for all three years (Figure 8). Meanwhile, correlation between NDBI and LST becomes less stable when NDBI increases. And in urban areas where NDBI is larger than 0, the linear relationship barely exists.

(a) NDBI 2001   (b) NDBI 2006   (c) NDBI 2010

(d) %ISA 2001   (e) %ISA 2006   (f) %ISA 2010
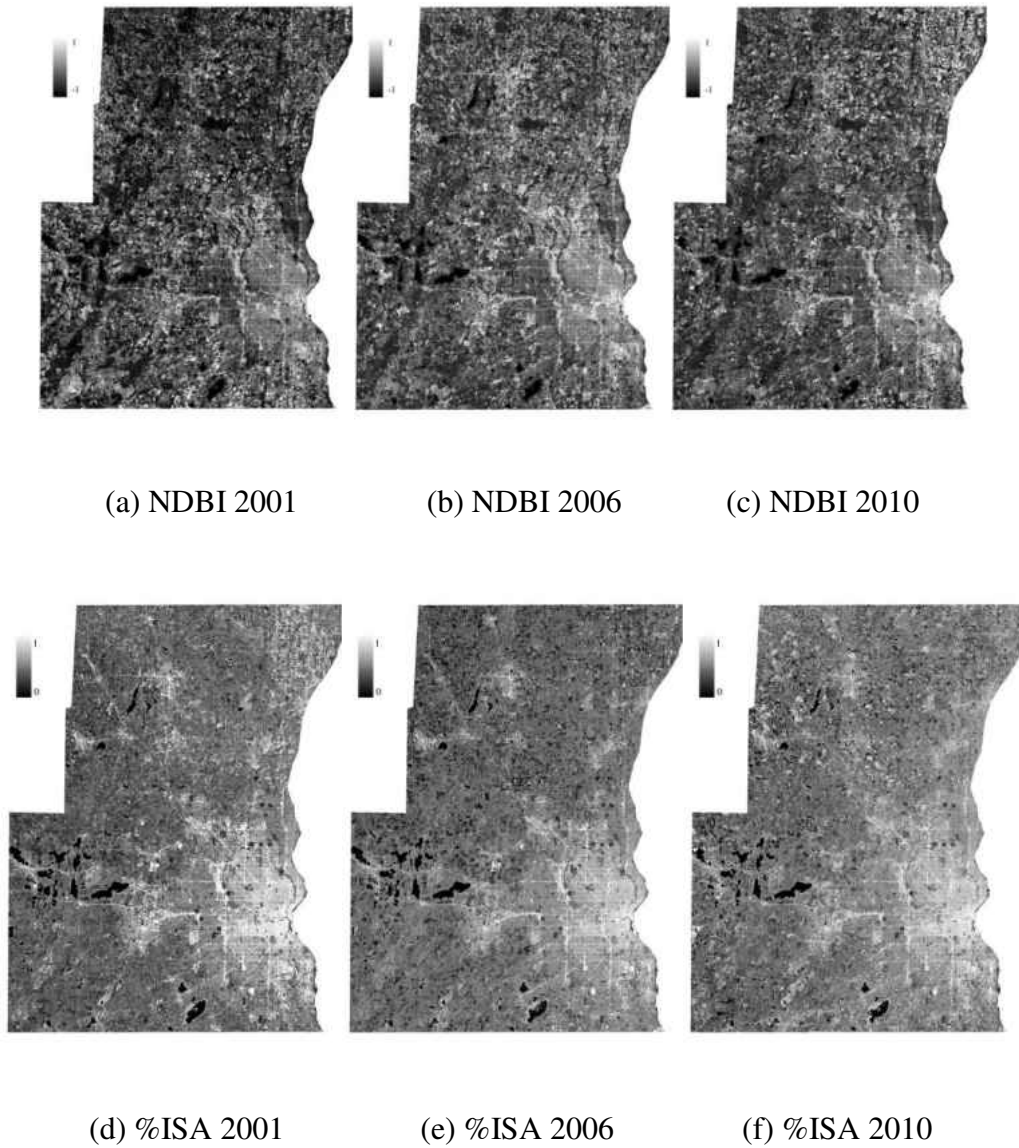
Figure 6 NDBI (a, b and c) and %ISA (d, e and f) of the study area
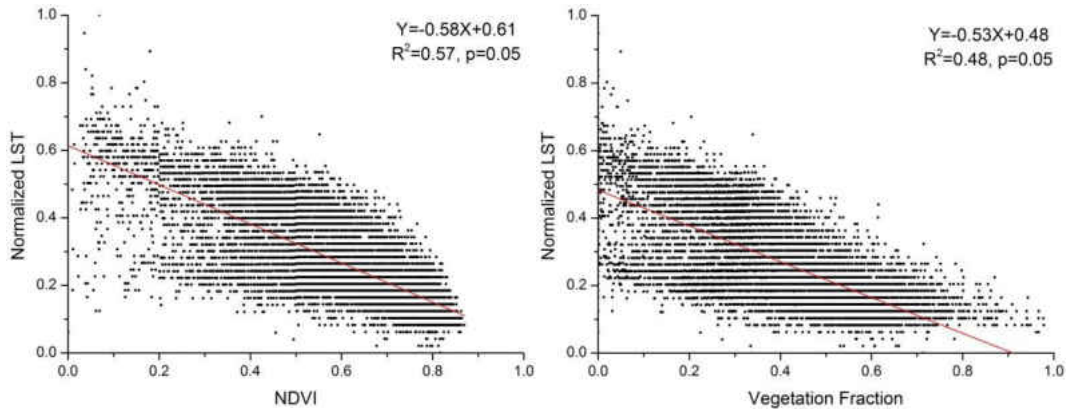
(a) 2001
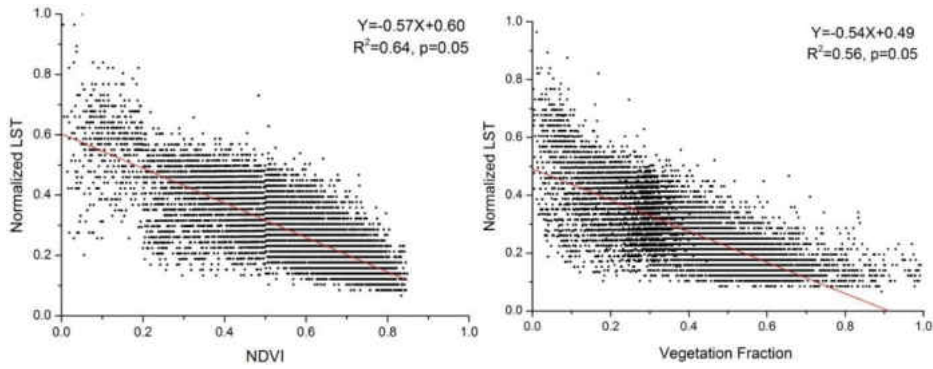
(b) 2006
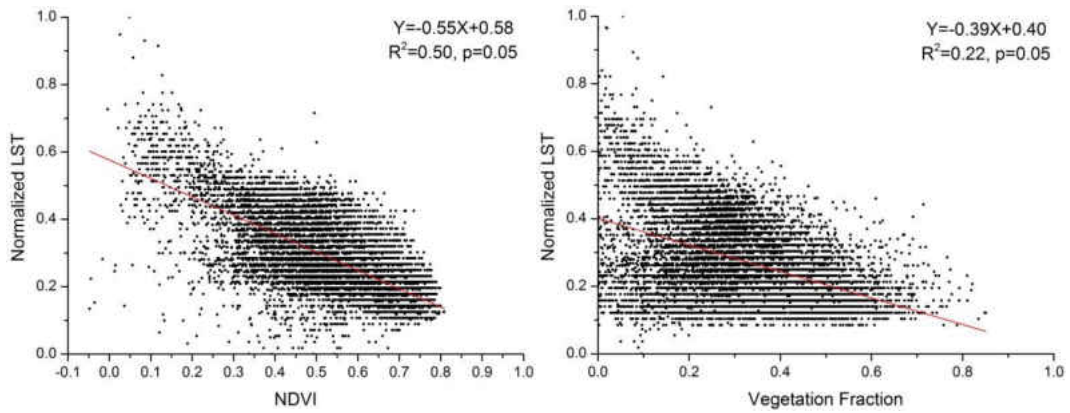
(c) 2010

Figure 7 Linear regression Between NDVI, %GV and LST
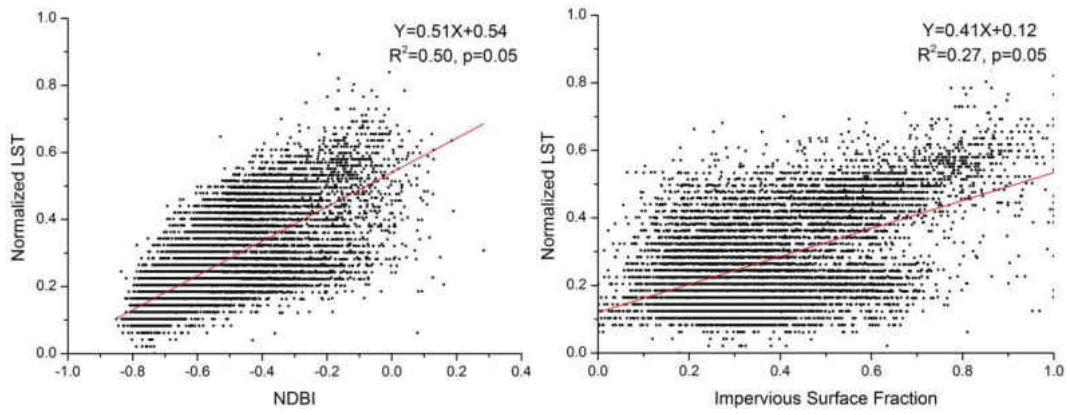
(a) 2001
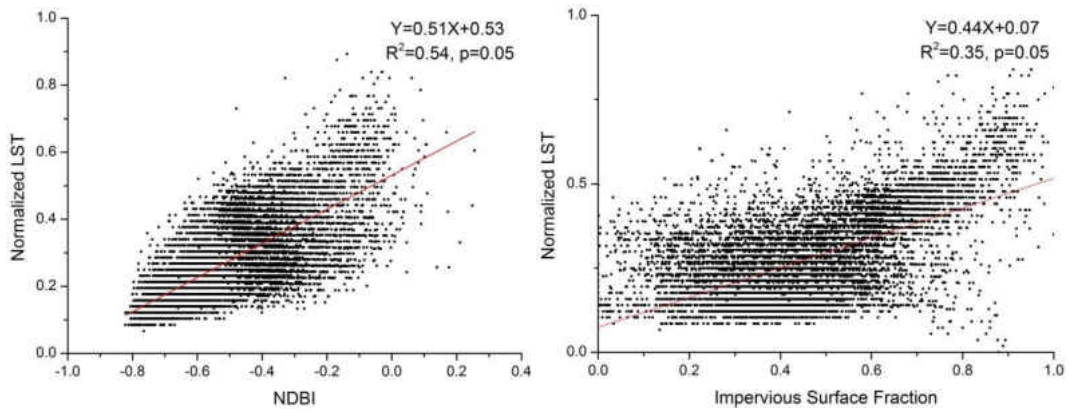
(b) 2006
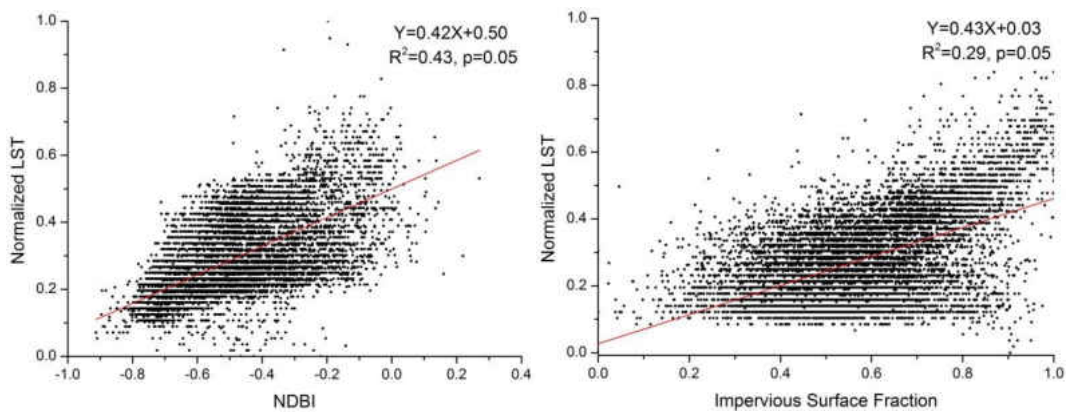
(c) 2010

Figure 8 Linear regression between NDBI, %ISA and LST

29

2.4.3 Analysis of LST variation within the study area

Comparative analysis between spectral indices and land cover fractions indicated that correlation between LST and its indicators grows weaker when vegetation abundance decreases. In order to quantify this trend, standard deviations of LST at different intervals of %GV were calculated (Table 2). Results indicate that LST is stable in fully vegetated areas with lower standard deviations and becomes unstable as vegetation loses its domination. As the standard deviations achieve their peak values in non-vegetated areas, LST is difficult to predict.

Table 2 Standard deviation of LST (K) at different intervals of %GV

%GV	0.000~0.250	0.251~0.500	0.501~0.750	0.751~1.000
2001	4.931	3.918	2.115	1.420
2006	1.418	0.996	0.568	0.505
2010	1.442	0.847	0.487	0.252

Following the V-I-S model proposed by Ridd (1995), soil and impervious surface are two land cover types in non-vegetated areas. Thus, large variation of LST in non-vegetated areas must be related to soil or impervious surfaces. However, only very limited numbers of pixels dominated by soil (%Soil>0.8) can be found (Figure 9), since most rural areas within the study area are covered by vegetation in summer, and urban areas are dominated by impervious surfaces. Further, LST of the pixels with high %Soil vary in a small range (Figure 9), which means soil is not responsible for the large LST variation.
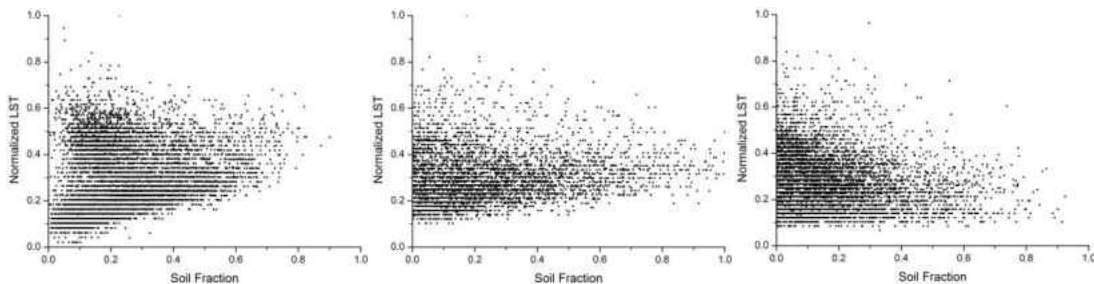
30

Figure 9 Scatter plot of LST and %Soil

Conversely, LST varies dramatically when %ISA is larger than 0.7 (Figure 8), which indicates

that impervious surfaces may lead to the large variation of LST in urban areas. In order to verify

these relationships, BCI was employed to identify impervious surfaces from soil. The scatterplot

of BCI and LST (Figure 10) indicates that BCI has a fine linear relationship with LST until it

exceeds 0. Given the report (Deng and Wu, 2012) that impervious surface is the main land cover

type when BCI is larger than 0, it is safe to claim that impervious surface is the land cover which

is responsible to the large LST variation in non-vegetated areas.
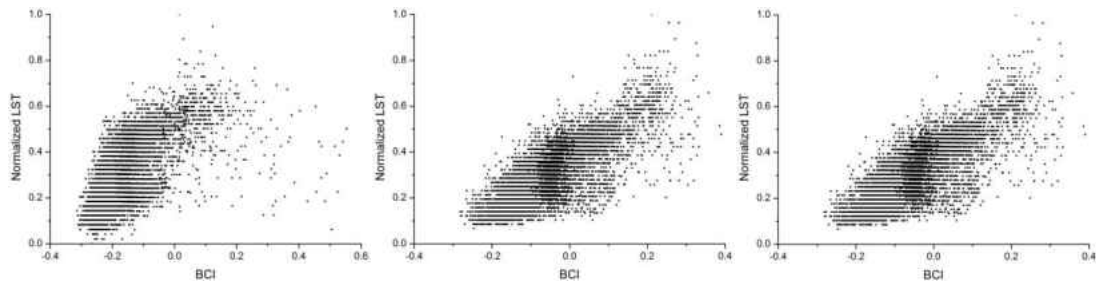
(a) 2001   (b) 2006   (c) 2010

Figure 10 Scatter plot of BCI and LST

The spatial distribution of high %ISA pixels (%ISA>0.7) was also explored through categorizing

pixels by temperature. Pixels with 0.7 or larger %ISA within the central part of the city of

Milwaukee were first selected from each image. Then normalized LST was employed to divide

them into three groups: pixels with 0.3 or lower normalized LST are low temperature pixels

(LTPs); high temperature pixels (HTPs) are those with 0.7 or higher normalized LST; the rest are

medium temperature pixels (MTPs) with normalized LST varies between 0.3 and 0.7. According

to Figure 11, LTPs (blue pixels) distribute along the shore area of Lake Michigan. HTPs (red

pixels) and MTPs (green pixels) mainly distribute along roads and in downtown area with clustered buildings. However, the spatial distribution of HTPs is more compact. They are found in the center of high %ISA areas while MTPs are more scattered along roads and in residential areas where vegetation can be frequently found. These spatial patterns of pixels with different LST seem to be relevant to the neighboring environment, as each group of pixels has distinct surrounding land covers.

(a) 2001   (b) 2006   (c) 2010

Figure 11 Spatial Distribution of high %ISA pixels

2.4.4 Influence of neighboring environment on LST

For quantifying the intensity of SUHI and the influence of neighboring environment on LST, $\overline{LST}_d$ and $\overline{NDVI}_d$ were calculated for LTPs, MTPs and HTPs respectively (Table 3). It is noteworthy that $\overline{NDVI}_d$ was not calculated for LTPs as most of them are found along the shore of Lake Michigan and surrounded by pure water pixels. Since it is clear that the low LST of LTPs is the result of the cooling effect of water, $\overline{NDVI}_d$ was not calculated for them as it is utilized to relate SHUI intensity to the cooling effect of vegetation. For all three years, high %ISA pixels have higher LST than their neighbors as $\overline{LST}_d$ is always positive. As the LST

32

increases, $\overline{LST}_d$ rises accordingly, indicating that SUHI intensity of HTPs is higher comparing to MTPs and LTPs. $\overline{NDVI}_d$ is negative in all three years, which proves that MTPs and HTPs are surrounded by pixels with higher vegetation abundance comparing to themselves. Higher absolute values of $\overline{NDVI}_d$ for MTPs indicates that vegetation abundance of their neighboring pixels is higher than that of pixels surrounding HTPs. It demonstrates that vegetation is a key factor correlates with the LST of high %ISA pixels in urban areas: although having similar %ISA, MTPs have lower LST than HTPs do as they are surrounded by more abundant vegetation.

Table 3 $\overline{LST}_d$ and $\overline{NDVI}_d$ for high %ISA pixels

Year	$\overline{LST}_d$			$\overline{NDVI}_d$	
	LTPs	MTPs	HTPs	MTPs	HTPs
2001	0.743	0.815	1.819	-0.074	-0.037
2006	0.091	0.100	0.444	-0.072	-0.037
2010	0.035	0.055	0.342	-0.061	-0.035

In order to verify the influence of the neighboring environment on LST, an average filter method was employed. In this study, five filter window sizes were applied and the original image was considered the result of an average filter with a 1x1 pixel window. Then linear regression between %ISA and LST was carried out utilizing five thousand pixels randomly selected from high %ISA pixels. For all three years, R-squared values increased dramatically as the average filter was applied to the original image and achieved its peak when a 5x5 pixel window was utilized (Figure 12). Then R-squared values dropped continuously as the size of the window increased and fell to a minimum as a window of 11x11 pixel was applied.

(a) 2001   (b) 2006   (c) 2010
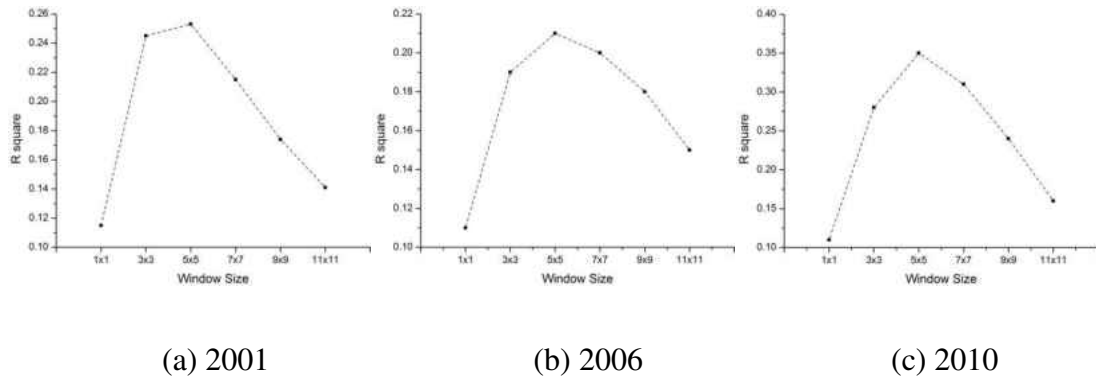
Figure 12 R squares ($p<0.05$) of linear regression between recalculated %ISA and LST

2.5 Discussion

Correlating with LST, spectral indices and land cover fractions have played an important role in the study of SUHI with remotely sensed data. Existing studies have reported that land cover fractions have better performance in predicting LST. Weng et al.(2004) reported that %GV has better performance than NDVI at various spatial scales in summer. Yuan and Bauer (2007) also reported %ISA in urban areas has better linear relationships with mean LST than NDVI at all four seasons. However, comparative analysis in my study indicates that spectral indices (NDVI and NDBI) have better performance as indicators of LST than their corresponding land cover fractions (%GV and %ISA). Giving the opposite results, better performance of spectral indices can be explained from three aspects: (1) NDVI and NDBI were designed based on the most representative bands of vegetation and buildings where their reflectance is dramatically different from other commonly existing land covers on the earth's surface. Therefore, less influence from other land cover types is taken into account when NDVI and NDBI are calculated; (2) the accuracy of land cover fractions depends on the endmember selection, which is a complex and relatively subjective process. Although many methods have been proposed for endmember

34

selection (Rashed et al., 2001; Small, 2001; Van Der Meer & Jong, 2000; Smith et al., 1985), there is still no consensus on an optimal and standard procedure of endmember selection due to the complexity of land cover reflectance spectra. Consequently, uncertainty exists in land cover fractions retrieval as it is not certain that endmembers selected from the image can accurately represent pure land covers in the real world; (3) LSMA assumes the spectrum of each pixel is a linear combination of the spectra of all endmembers within the pixel. However, as a simplification of the true situation, it cannot perfectly explain the real combination of spectra and always bring errors into the result of spectral mixture analysis. In other words, land cover fractions are always affected by the accuracy of endmember selection and spectral model utilized to unmix spectra, while NDVI and NDBI are two simple but reliable indices which indicate the abundance of vegetation and buildings. Thus, it is reasonable that spectral indices perform better than landcover fractions in LST estimation.

Conversely, large LST variations were found in less- and non-vegetated areas. It is not surprising that impervious surfaces are responsible for this phenomenon since: (1) soil is covered by vegetation in rural areas in summer and barely exists in urbanized areas; (2) impervious surfaces include a series of materials which could have different thermal properties. Although Yuan and Bauer (2007) argued that %ISA has strong correlation with mean LST, it is arbitrary to claim that high %ISA pixels always have high LST; and (3) existing studies have confirmed that vegetation and water have the ability to cool their surrounding environment (Jauregui, 1991; Spronken-Smith and Oke, 1998; Shashua-Bar and Hoffman, 2000; Munn et al., 1969; Ackerman, 1985). Thus, neighboring environment is another factor which also affects LST of impervious surfaces and leads to low LST in high %ISA areas.

As high %ISA pixels were categorized by normalized LST and located in the study area, neighboring effect was suspected as the origin of the large variation of LST due to the spatial patterns of pixels with different LST. LTPs were mostly found along the shore of Lake Michigan. Their low LST can be explained by the cooling effect from the lake. The cooling process of large water bodies occurs when regional winds blow from lake to land. Moreover, when temperature inland is higher than that above water on sunny days, gradient winds also blow from land to lake and bring hot air out of the urban areas. However, the cool air from a lake could be easily modified by warmer surfaces such as roads, pavements and building walls. Therefore, direct cooling effects of a lake on adjacent urban areas have been confirmed, but are limited to the urban areas close to the lakeshore (Munn et al., 1969; Ackerman, 1985). MTPs distribute linearly along roads and within residential areas while LTPs are clustered in the center of downtown or business areas around the city. The clear difference of spatial distribution between HTPs and MTPs may be considered as the outcome of vegetation's cooling effect. In residential areas where grass and trees are widely planted, surface temperature of impervious surfaces are relatively lower than downtown and business areas where lots of buildings are clustered and less vegetation exists. MTPs can also be found along roads, and this could also be explained by the vegetation planted in the open fields along the roadside. In other words, LST of impervious surfaces is relevant to their surrounding environment. Pixels surrounded by vegetation or water could have lower LST and SUHI intensity comparing to those with similar %ISA but surrounded by other high %ISA pixels. Calculation of $\overline{LST}_d$ and $\overline{NDVI}_d$ provided support from quantitative perspective for this claim.

Average filter method was proposed to provide a way to include neighboring effect when %ISA is utilized to estimate LST. According to the results, R-squared values changed with one pattern as the size of the window increases for all three years. This indicates that neighboring environments do have an influence on the prediction of LST. %ISA has much better performances in predicting LST when the influence of surrounding pixels is considered. However, accurate definition of the neighboring environment is crucial. In other words, the output of this method is sensitive to filter window size. As the size increased from 1x1 pixel, R-squared values increased at the beginning and started to decrease when the size became larger than 5x5 pixels. I contend this phenomenon justifies the existence of neighboring effect, or more specifically, the cooling effect of vegetation within the study area. Since soil can barely be found within the area of interest, abundance of vegetation and impervious surfaces decides LST. When mean %ISA between a pixel and its close neighbors is calculated, influence of surrounding vegetation is taken into account. Thus, it is natural to expect a better estimation of LST. However, when the definition of neighborhood is extended, or in other words, the size of the filter window continues to increase, it is more likely that more pixels with high %ISA are included, given that more than half of the study area is urbanized at different levels. Since the correlation between %ISA and LST has been proven poor, especially in high %ISA areas, increasing the size of filter window arbitrarily could cover up the influence on LST from surrounding vegetation and thus lead to lower R-squared values. According to the results of my study, a 5x5 pixel is the proper size for the filter window. However, I do not think this is a universal answer and it could vary depending on the land cover composition within a specific area.

2.6 Conclusion

This study first examined the performance of spectral indices and land cover fractions as indicators of LST in the Milwaukee metropolitan and surrounding rural areas utilizing an ETM+ and TM images acquired from three summers. Results indicate that spectral indices have stronger linear relationships with LST, while the relationships among land cover fractions and LST surfers from the uncertainty brought by endmember selection and spectral mixture analysis. Large variations of LST in urban areas were also found and investigated. Impervious surfaces were responsible for the unstable LST, whereas soil can barely be found within the study area and does not play a vital role. Further analysis indicates that LST of high %ISA pixels are dramatically affected by the surrounding environment. Although %ISA as a single indicator of LST may not be reliable, its performance can be enhanced as the influence of neighboring environment is considered during the estimation of LST. Despite what has been revealed in this study, I realize that the conclusions are all based on one single area at one scale. Further studies in other urban areas at different scales should be done to further verify the conclusions of this research.

CHAPTER 3 EXAMINING HUMAN HEAT STRESS WITH REMOTE SENSING TECHNOLOGIES

3.1 Introduction

Global climates has become warmer in the past century, and this trend is projected to continue over at least the next one hundred years (Pachauri et al., 2014). Many studies have agreed that the

number of heat waves and concomitant adverse influence on human health (and even survival) are anticipated to expand as the global temperature increases (Meehl and Tebaldi, 2004; Patz et al., 2005). More than seventy thousand lives across Europe were taken by a heat wave that occurred in August 2003 (Robine et al., 2008). Another heat wave in Chicago killed more than seven hundred people during July 1995 (Semenza et al., 1996). Approximately ten thousand people were also killed by a heat wave across the US in 1980 (Sheridan and Kalkstein, 2004). Meanwhile, recent studies have reported that population around the world has become more resilient to heat over time through physiological, infrastructural and technological adaption, yet the substantial risks of heat mortality remain, as extremely hot weather appears more frequently (Bobb et al., 2014; Hondula et al., 2015). Addressing human heat stress spatially has never been such an important task to prevent (or at least minimize) heat associated morbidity and mortality.

Heat stress is not only associated with temperature, but also other factors such as physiological condition and relative humidity. In order to relate physiological heat strain perceived by individuals to the heat stress one is exposed to, many studies have focused on estimation of the stress originating from surrounding environments or climate through a single heat stress index (Haldane, 1905; Hill et al., 1916; Dufton, 1929; Belding and Hatch, 1955; McKarns and Brief, 1966; Gonzales et al., 1978; Frank et al., 1996; Wallace et al., 2005). Heat stress indices proposed so far can be categorized into three groups: rationale indices, empirical indices and direct indices (Epstein and Moran, 2006). Calculation of the first two groups is usually complicated and requires both environmental and physiological data, which is beyond the scope of this research project. However, direct indices which are based on the measurement of basic environment variables are easy to implement, and thus have been widely utilized to address heat stress under various

circumstances. Houghton and Yaglou (1923) proposed effective temperature (ET), which is considered as the first direct heat stress index. It was established to provide a measurement of temperature and humidity on human comfort. As the most widely utilized heat stress index, wet-bulb globe temperature (WBGT) was developed by the US Navy as part of a study associated with heat related injuries during military training (Yaglou and Minard 1957). Coefficients in WBGT were determined empirically and no physiological variables were needed to calculate the index. In spite of the simplicity of WBGT, its limitation lies in applicability across a broad range of environments, due to the inconvenience of black-bulb temperature measurements. Discomfort index (DI) is another heat stress indicator proposed by Thom (1959) and was adjusted by Sohar et al. (1963). It requires only dry-bulb and wet-bulb temperature as the input and has proven to be a reliable direct heat stress index due to its strong correlation with effective temperature and its physiological significance (Tennenbaum et al., 1961). Heat load of two cities in Israel was addressed by DI (Eyre et al., 1982). Shapiro and Seidman (1990) also employed DI as an indicator of heat stress when discussing the prevention of heat stroke. Different from heat stress indices, bioclimatic comfort employs multiple environmental and personal parameters to evaluate heat environment (Oliveira and Henrique, 2007; Cetin, 2015; Cetin et al., 2016). Despite all the work done to address heat stress, indicators are usually measured at specific sites where individuals were exposed to extreme heat stress due to their occupations, such as construction workers and soldiers. However, addressing heat stress only at scattered sites may not be sufficient, since any citizens exposed to high temperature can be threatened by heat stress, and extreme hot weather has appeared more frequently within large areas such as a country or even across a whole continent (Meehl and Tebaldi, 2004; Patz et al., 2005; Robine et al., 2008). Spatial information is urgently needed for addressing heat stress across continuous space.

Remotely sensed data with abundant spatial information and flexible temporal resolution have long been utilized to study urban heat islands (UHI), which refer to the phenomenon that urban are usually found to have higher temperature comparing to surrounding rural areas, due to surface and atmospheric modifications brought by urbanization (Voogt and Oke, 2003). However, remotely sensed data have never been introduced to address heat stress since only land surface temperature (LST) can be collected by remote sensors. Since LST could be dramatically different from air temperature(which is a key factor affects the heat stress individuals experience), many studies address the relationship between LST and air temperature (Stoll and Brazel, 1992; Ben-Dor and Saaroni, 1997; Hafner and Kidder, 1999; Kloog et al., 2012; Hill, 2013; Shi et al., 2016). However, due to the complexity of surface atmospheric condition, only empirical models can be developed. Nevertheless, addressing the relationship between LST and air temperature is possible, and thus provides a potential tool to study heat stress spatially with remotely sensed data.

This research aimed to address human heat stress across continuous space at the state level with remotely sensed data. Although various heat stress indicators have been proposed to address heat stress, many of them cannot be calculated with remotely sensed data. Thus, specific principles were followed before DI was chosen as the heat stress indicator of this study: (1) the indicator can be calculated from variables that can be retrieved (directly or indirectly), from remotely sensed data; and (2) The index must have been proven by published studies to be effective at indicating human heat stress. In order to retrieve DI, empirical models were first established to connect LST with air temperature, which was considered as dry-bulb temperature in this study. Then wet-bulb temperature was retrieved from dry-bulb temperature and relative humidity. As

41

DI was calculated from dry-bulb and wet-bulb temperature, its spatial distribution was compared with LST. Finally, correlation analysis between LST, normalized difference vegetation index (NDVI), normalized difference built-up index (NDBI) and DI was done to compare the spatial distribution of DI and LST, and address the significance of DI as an indicator of heat stress within continuous space.

3.2 Study area and data

The State of Wisconsin, which lies in the north-central region of the United States, was chosen as the study area for this research. Wisconsin is within the latitudes of 42°37'N-47°5'N and longitudes of 86°46'W-92°53'W, and has a geographic area of 169,639 km^2, divided into seventy-two counties (Figure 13). Although the state has a fairly large area, more than 68% of the population resides in several urban areas including Milwaukee (the most populated city), Madison (state capital) and Green Bay. Wisconsin has experienced fast population growth during the last several decades. The population of Wisconsin increased from 4.89 million in 1990 to 5.69 million in 2015, which is an increase of nearly 16% in twenty-five years, and this trend is expected to continue into the future. Further, analysis of weather trend data done by the Wisconsin Initiative on Climate Change Impacts (WICCI) indicates that Wisconsin has become warmer over the last 60 years (Human Health Working Group, 2011).

Figure 13 Study area

In this study, three MODIS daytime land surface temperature images (product of MOD11A1, daily land surface temperature with 1km spatial resolution) acquired on 14 July 2008 (hereinafter "7/14"), 26 August 2010 (hereinafter "8/26") and 6 August 2012 (hereinafter "8/6",Figure 14) were obtained from the United States Geological Survey (USGS) to retrieve dry-bulb temperature. Specifically, 6 August 2012 as a cloudless day was firstly selected since the temperatures in the upper Midwest of the United States were notably high in summer 2012. Then the other two cloudless days were selected following several principles: (1) The other two summers should be as close to the temperatures in 2012 as possible and temporal resolution should remain the same among the different years; (2) Selected days should have as few clouds as possible, ideally cloudless; (3) While the second rule is followed, selected days should be as close to August 6th as possible in each year. MODIS NDVI data (product of MOD13A2, vegetation indices with 1 km spatial resolution) for the study area were collected to examine the correlation between DI and vegetation abundance. NDBI, on the other hand, is a measurement of impervious surfaces abundance employed in this research to address the connection between DI and urbanization.

43

MODIS reflectance data from band 2 (near-infrared) and band 6 (shortwave infrared) were acquired to retrieve NDBI for the study area.
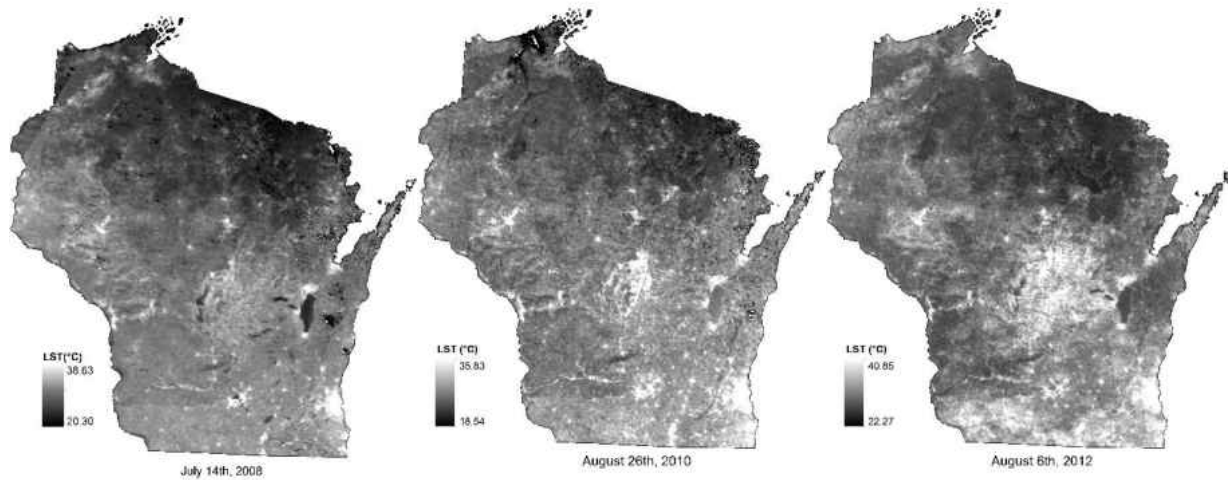
Figure 14 LST of the study area

Relative humidity data at 2 m height for the study area on the same days (Figure 15) were obtained from North America Regional Reanalysis (NARR) to retrieve wet-bulb temperature. Air temperature and wet-bulb temperature acquired at 11:00am for the same days from forty-nine meteorological stations (uniformly distributed across the study area) were collected from the National Oceanic and Atmospheric Administration (NOAA) to obtain dry-bulb temperature empirically and carry out the accuracy assessment for retrieved dry-bulb and wet-bulb temperature.
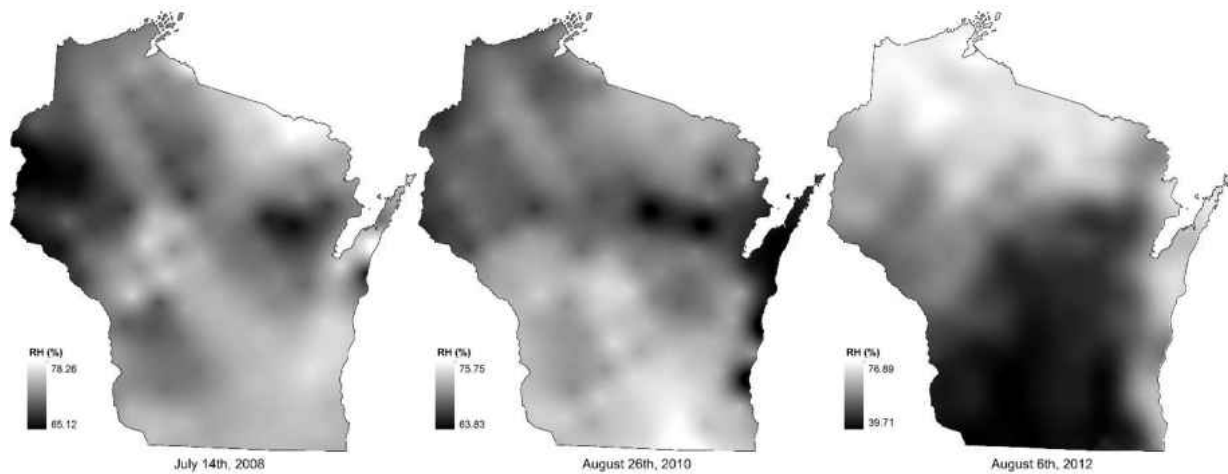
Figure 15 Relative humidity of the study area

3.3 Methods

3.3.1 Retrieval of DI

DI was originally proposed by Thom (1959) and was adjusted by Sohar et al. (1963) as follows:

$$\text{DI} = 0.5T_a + 0.5T_w \qquad (23)$$

where T_a (°C) is dry-bulb temperature; T_w (°C) is wet-bulb temperature.

Retrieval of Dry-bulb Temperature

Dry-bulb temperature refers to the air temperature measured by a thermometer exposed to the air, but shielded from moisture and radiation. In this study, dry-bulb temperature of the study area, which was considered equal to air temperature, were retrieved from MODIS land surface temperature data at 1km spatial resolution.

Trying to connect land surface temperature to air temperature, many efforts have been made to find a numerical relationship between them (Prihodko and Goward, 1997; Cresswell et al., 1999; Vancutsem et al., 2010). However, only empirical models were built due to the complexity of the energy transmission in the lowest atmosphere layers. In this study, three regional models addressing the statistical relationship between land surface temperature and dry-bulb temperature were first established. Specifically, thirty-four stations were randomly selected from forty-nine NOAA meteorological stations within the study area. Air temperature from these stations were employed to establish empirical models between LST and dry-bulb temperature (Table 4). Air temperature from the remaining fifteen stations were then utilized to assess the accuracy of empirical models. Specifically, root mean square error (RMSE) was utilized for accuracy assessment of dry-bulb temperature for each year. It can be expressed as follows:

$$\text{RMSE} = \sqrt{\frac{1}{N}\Sigma_1^N(T_{a_i} - T_{a_i}{'})^2} \qquad\qquad (24)$$

where T_{a_i} is dry-bulb temperature retrieved from LST of the study area; $T_{a_i}{'}$ is the dry-bulb temperature acquired by in-situ measurement from meteorological station i. N is the total number of meteorological station employed for accuracy assessment (and equals fifteen in this study).

Table 4 Models for dry-bulb temperature retrieval

Date	Model (°C)	R^2 ($p<0.05$)	RMSE (°C)
July 14th, 2008	Ta*=0.70LST+4.01	0.61	1.34
August 26th, 2010	Ta=1.29LST-2.21	0.62	0.86
August 06th, 2012	Ta=0.29LST+19.11	0.59	0.69

*Ta is dry-bulb temperature

It is worth of noting that MODIS daytime land surface temperature data were acquired by the Terra satellite at 10:30 am local time. Since air temperatures were acquired once an hour by NOAA meteorological stations, data acquired at 11:00 am at each station were utilized to develop the models.

Retrieval of Wet-bulb Temperature

The wet-bulb temperature is the temperature a parcel of air would have if it were cooled to saturation (100% relative humidity) by the evaporation of water into it, with the latent heat being supplied by the parcel. Wet-bulb temperature is measured by a thermometer wrapped in cloth, which is kept wet with distilled water. Considering the complexity of the measurement of wet-bulb temperature, it is not practical to collect wet-bulb temperature over continuous space, especially across a large geographic area, such as the State of Wisconsin. However, there is no existing study which has established the statistical relationship between air temperature and wet-bulb temperature through a univariate model.

While acknowledging the difficulty of measuring wet-bulb temperature, this research employed a method proposed by Stull (2011) to retrieve wet-bulb temperature from relative humidity and air temperature over the study area. This empirical method is expressed by the following formula:

$$T_w = T_a * atan[0.151977(RH + 8.313659)^{0.5}] + atan(T_a + RH) - atan(RH - 1.676331) + 0.00391838 * RH^{1.5} * atan(0.023101RH) - 4.686035 \tag{25}$$

where T_a (°C) is dry-bulb temperature; RH (%) is relative humidity; and T_w is the wet-bulb temperature. The applicability(i.e. valid range) of this model is mainly affected by three factors

47

(Stull, 2011): RH (%), air temperature (°C) and air pressure (kPa). In my research, air temperature varied between 18.06°C and 31.20°C, while RH varied between 39.71% and 78.26% for the three selected days. Both RH and air temperature were in the valid range of Stull's report. However, air pressure is another factor that can influence model accuracy . As the ideal air pressure of this model is 101.325 kPa, the model can still be reliable when air pressure is above 60kPa, but the accuracy decreases with the air pressure. As measured by all the employed weather stations in my research, average air pressure was 97.6kPa, 98.6kPa and 98.1kPa for 7/14, 8/26, and 8/6 respectively within the study area, and minimum air pressure was 95.4kPa. Since air pressure of the selected days was close to the ideal value, I judged the error as acceptable. Please refer to Stull's (2011) study for detailed discussion on the applicability and accuracy of the model.

It is also worth noting that the original spatial resolution of NARR relative humidity data is approximately 32km, which varies at different locations. Kriging interpolation was used to downscale the spatial resolution to 1km within the study area to keep spatial resolution consistent with dry-bulb temperature.

3.3.2 Correlation between NDVI, NDBI and DI

As DI was retrieved, its correlation with typical land covers (vegetation and impervious surfaces) were also examined to compare its spatial distribution with the spatial distribution of LST, which has been proved to have stable correlation with vegetation and impervious surface abundance (Weng et al., 2004; Yue et al., 2007; Deng and Wu, 2012; Black and Stephen, 2014; Rhee et al.,

48

2014; Hao et al., 2016). Two spectral indices were employed to address the abundance of different land covers. Specifically, NDVI is a spectral index which indicates vegetation abundance through normalization of reflectance differences within the red and near-infrared bands. Inspired by NDVI, NDBI was developed to address abundance of built-up areas by normalizing differences of reflectance between the near-infrared and shortwave infrared bands (Zha et al., 2003). NDBI can be considered as an indicator of urbanization, and has a positive correlation with impervious surface abundance. NDVI and NDBI were calculated through the following equations.

$$NDVI = \frac{NIR-RED}{NIR+RED} \tag{26}$$

$$NDBI = \frac{SWIR-NIR}{SWIR+NIR} \tag{27}$$

where RED, NIR and SWIR are the reflectance of red, near-infrared and shortwave infrared bands respectively. As NDVI and NDBI were retrieved within the study area for all three selected days, their correlations with DI were also explored by ten thousand non-water pixels randomly selected from each imagery. Ordinary Least Squares (OLS) was employed to address the linear correlation between NDVI, NDBI and DI.

3.4 Results

3.4.1 Spatial distribution of LST and dry-bulb temperature

LST retrieved from MODIS can be utilized as a direct indicator of surface UHI. LST varied between 20.30°C-38.63°C, 18.54°C-35.83°C and 22.27°C-40.85°C on 7/14, 8/26 and 8/6 respectively. Although min. and max. values of LST varied in different years, high values (third quartile, Q_3) were found clustered in similar areas where the major cities (Milwaukee, Madison

49

and Green Bay) of Wisconsin are located (Figure 14). Surface UHI effect can be easily observed for all three years through the obvious contrast of LST between rural and urban areas. As the most populated area of the state, the Milwaukee metropolitan area (located in the southeastern part of the study area) is especially evident.

In order to retrieve dry-bulb temperatures from the study area on selected days, three empirical models were first established by regression analysis between LST and air temperature measured at meteorological stations (Table 4). Dry-bulb temperatures varied between 18.35°C-31.20°C, 18.06°C-26.46°C and 25.84°C-29.69°C on 7/14, 8/26 and 8/6 respectively (Table 5). Spatial distribution of dry-bulb temperature for the study area is shown in Figure 16. For all three years, high dry-bulb temperatures (Q_3) can be found in highly urbanized areas where high LST (Q_3) was also found.
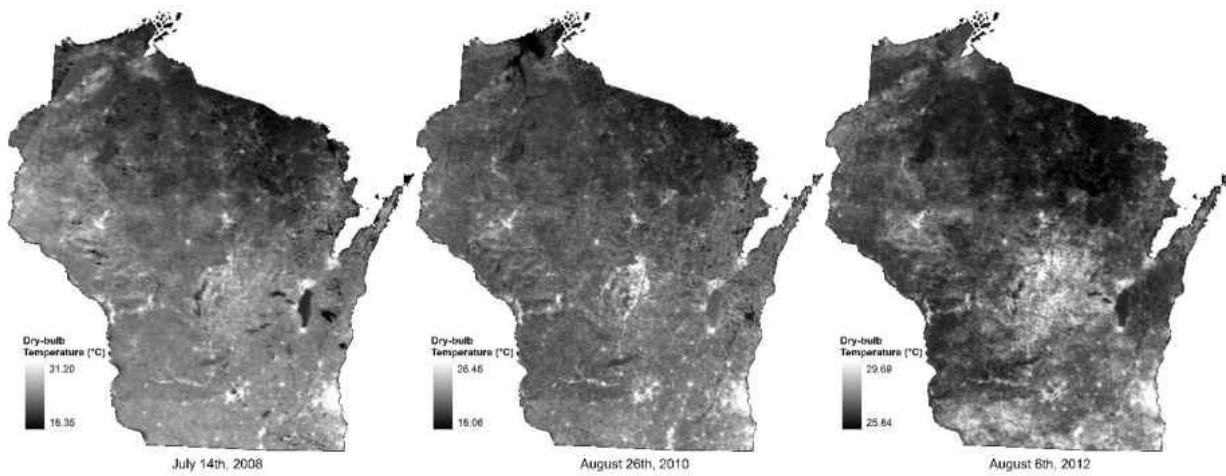
Figure 16 Dry-bulb temperatures in the study area

3.4.2 Retrieval of wet-bulb temperature and DI

As the input for equation 23, relative humidity plays an important role in the retrieval of wet-bulb temperature. Spatial distribution of relative humidity follows a similar pattern for 7/14 and 8/26 (Figure 15A and 15B): (1) High values (Q_3) occurred in the southern part of the state and along the shore of Lake Michigan. Northwestern parts of the study area (mostly covered by forests) also had high relative humidity (Q_3); (2) Low values (first quartile, Q_1) were found in the mid-eastern part of the state for both years. Meanwhile, low values (Q_1) also appeared in the midwestern and peninsula area of the state on 7/14 and 8/26 respectively. However, the spatial distribution of relative humidity for 8/6 (Figure 15C) was different from the former two selected days: (1) Most of the northern part of the state was covered by high relative humidity (Q_3). Areas along the shore of Lake Michigan also had high values for relative humidity (Q_3); (2) Minimum value of relative humidity for 8/6 was 39.5%, which is much lower than that for the other two selected days (65.0% and 63.6%). Meanwhile, low relative humidity (Q_1) was mostly found in the southern portion of the study area, where high relative humidity (Q_3) occurred on the other two selected days.

Table 5 Descriptive statistics for dry-bulb temperature, wet-bulb temperature and DI

	Range (°C)			Mean (°C)			Standard Deviation (°C)		
	2008	2010	2012	2008	2010	2012	2008	2010	2012
T_a	12.85	8.40	3.85	22.13	20.51	26.94	1.53	0.87	0.51
T_w	12.11	8.00	7.21	18.52	16.90	20.64	1.47	0.93	1.49
DI	12.51	8.19	4.85	20.34	18.71	23.81	1.49	0.89	0.71

Wet-bulb temperature (Figure 17) was then calculated from equation 3. It varied between 15.21°C-27.32°C, 14.68°C-22.68°C and 17.62°C-24.83°C on 7/14, 8/26 and 8/6 respectively

(Table 2). Spatial patterns of wet-bulb temperature were consistent with dry-bulb temperature for

7/14 and 8/26. Urban areas (where impervious surfaces are clustered) had high wet-bulb

temperature (Q_3), while rural and natural land cover area located in the north of the study area

showed lower values (Q_1). However, due to the unique pattern of relative humidity, spatial

distribution of wet-bulb temperature for 8/6 (Figure 17C) was also different from the other two

selected days. With high relative humidity (Q_3), the northern part of the study area had high wet-

bulb temperature (Q_3). Although the Milwaukee metropolitan area and other urban areas with

high values (Q_3) occur in the middle and southern parts of the State, most areas with high wet-

bulb temperature (Q_3) for the other two days had relatively low values (Q_1) on 8/6.

Wet-bulb Temperature (°C)	Wet-bulb Temperature (°C)	Wet-bulb Temperature (°C)
27.32	22.68	24.83
15.21	14.68	17.62
July 14th, 2008	August 26th, 2010	August 6th, 2012
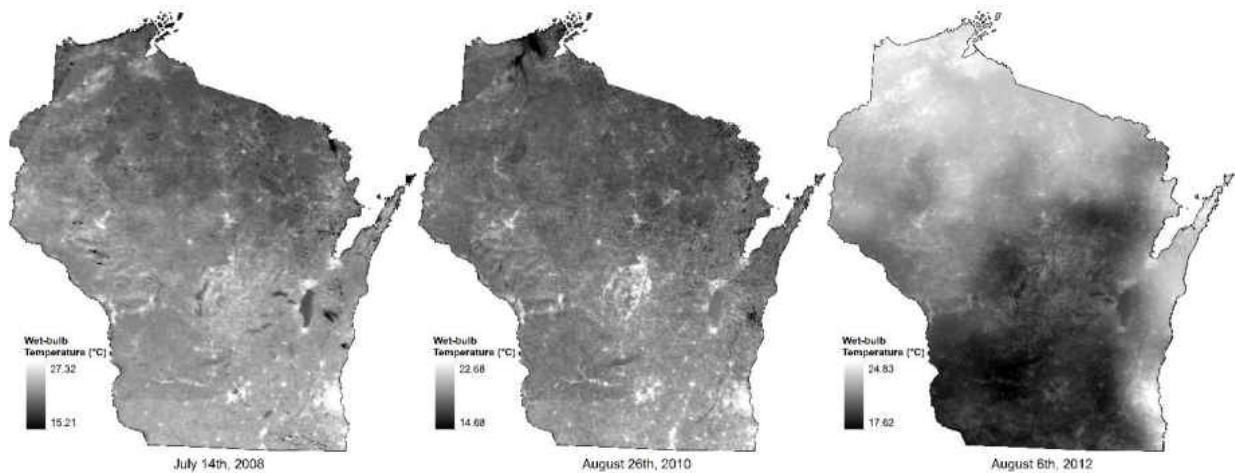
Figure 17 Wet-bulb temperatures in the study area

DI (Figure 18), which varied between 16.75°C-29.26°C, 16.38°C-24.57°C and 22.02°C-26.87°C

on 7/14, 8/26 and 8/6 respectively (Table 5), was calculated as the weighted summation of dry

and wet-bulb temperatures using equation 1. As DI has been widely applied to measure heat

stress, a criteria based on numerous observations associated with different population groups and

climatic conditions has been created to address environmental heat stress and thermal sensation

52

through a ranking system (Epstein and Moran, 2006): no heat stress can be sensed if DI is under

22°C (level 1); mild heat stress can be sensed by most people when DI is between 22°C and

24°C (level 2); heat stress is moderate with DI between 24°C and 28°C (level 3), people feel

very hot within this range and difficulties may be found when physical work is performed; heat

stress is severe if DI is above 28°C (level 4), people performing physical work are at high risk of

heat associated illness, such as heat exhaustion and heat stroke. Following this ranking system,

classified spatial distribution of DI are shown in Figure 19.
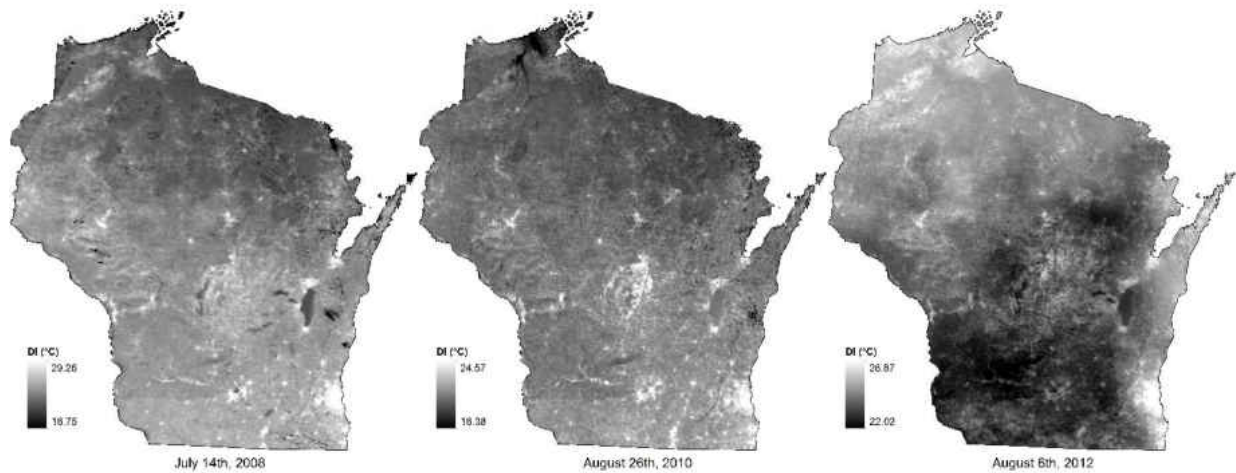
Figure 18 DI of the study area
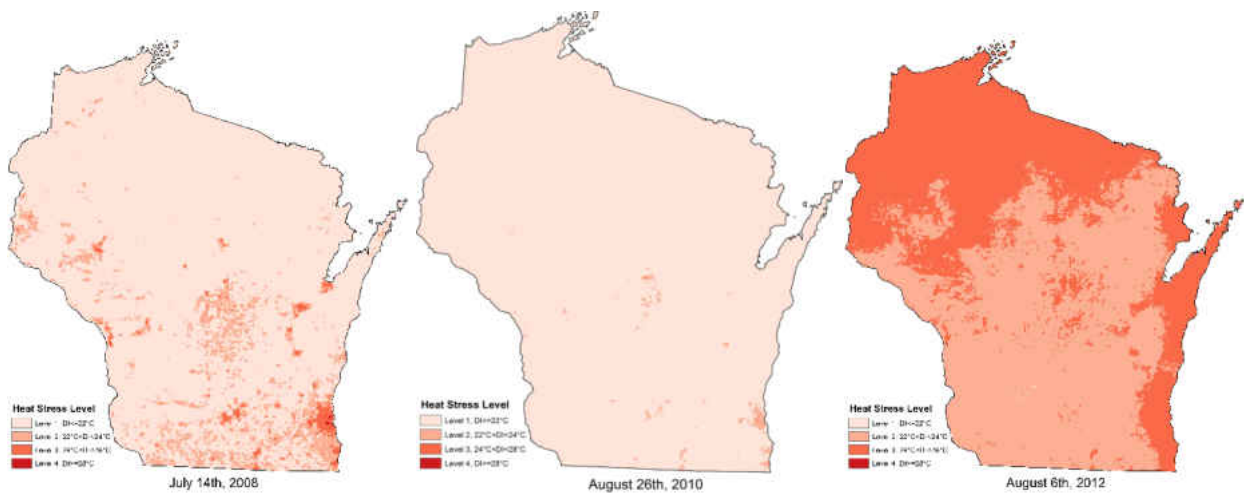
Figure 19 Classified DI in the study area

3.4.3 Correlation Analysis between LST, NDVI, NDBI and DI

Spatial distribution of NDVI and NDBI is mutually exclusive for all three selected days (Figure 20 and Figure 21). Ten thousand non-water pixels were then randomly selected from the study area for each selected day to carry out the correlation analysis. However, correlation between LST, NDVI, NDBI and DI varied dramatically from year to year (Figure 22), and will be discussed in the next section.
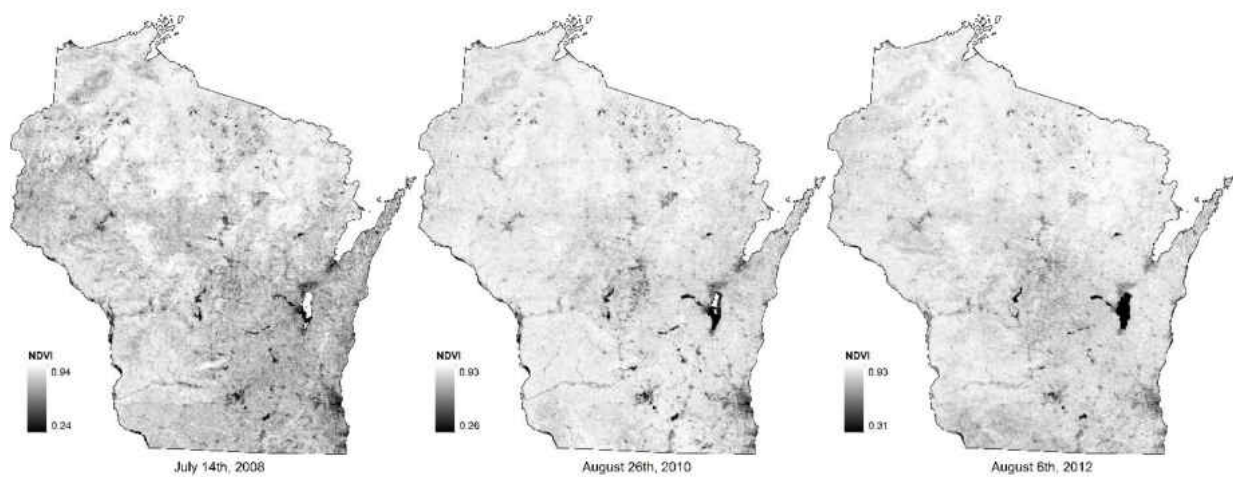
Figure 20 NDVI in the study area
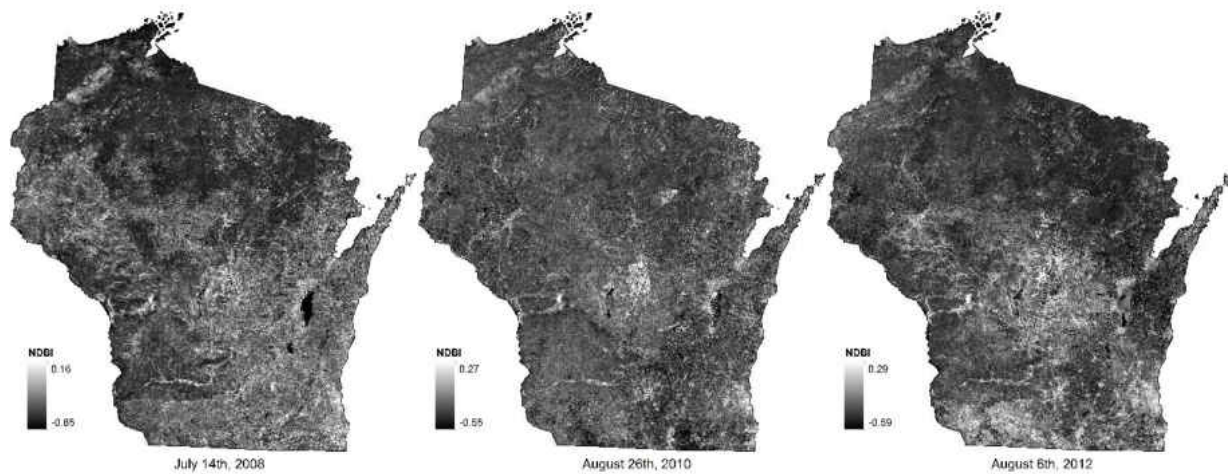
Figure 21 NDBI in the study area

3.5 Discussion

Calculation of DI begins from the measurement of dry-bulb and wet-bulb temperature. In

traditional applications, measurement is carried out by equipment deployed in the study area.

However, it is impossible to acquire data utilizing field equipment with 1km spatial resolution

for the study area. Thus, my research combined weather station measurements with remotely

sensed data to retrieve DI. Specifically, I utilized air temperature acquired by weather stations

within the study area to construct empirical models with LST for the selected days. Compared to

other reported methods, this approach is easier to implement as no atmospheric parameters or

land composition index is needed. It has been proven accurate with an average RMSE of $0.96^{o}C$

for air temperature on the selected days (Table 4). However, the shortcomings of this method are

obvious: (1) As the models were built statistically, the relationship between LST and air

temperature cannot be addressed; (2) Although accurate, correlation between LST and air

temperature revealed by this method is a snapshot based on the temperature of the study area for

55

a relatively short period (10:30 am to 11:00 am in this research), which makes these models

exclusive for this study and not for wider application to address the correlation between LST and

air temperature for any other time or areas.

As DI was retrieved from remotely sensed data, its spatial distribution was also revealed (Figure

18). It is not surprising to find that high DI (Q_3) areas were clustered in the most populated

regions of Wisconsin, such as Green Bay, Madison and the Milwaukee metropolitan area for all

three selected days. However, when the spatial distribution of DI of selected days were

compared, 8/6 is obviously unique. As high DI values (Q_3) were found in the northern part of the

study area for 8/6, low DI values (Q_1) were found for the other two selected days. As a result, the

northern part of the study area seems to be covered by haze on 8/6 (Figure 18C). I suspect

relative humidity was responsible for this outcome. Comparing the spatial distribution of relative

humidity (Figure 15), although high relative humidity (Q_3) can be found in north for 7/14 and

8/26, the southern part of the study area was mostly dominated by wet air. The situation for 8/6

was completely different: the southern part of the study area hadvery low relative humidity (Q_1),

but thenorthern part was mainly occupied by high relative humidity (Q_3). I thus investigated the

daily spatial distribution of relative humidity within a week of each selected day (three days

before and after the selected days, figures are not shown), and found that the spatial distribution

of relative humidity was similar during the two weeks of 7/14 and 8/26. However, the spatial

distribution of relative humidity during the week of 8/6 was dramatically different from the other

two. For the whole week, southern parts of the study area were occupied by low relative

humidity (Q_1) while the northern parts had high relative humidity values (Q_3). This difference of

spatial distribution of relative humidity led to the unique spatial distribution of wet-bulb temperature and DI on 8/6.

Despite LST having long been the main indicator of surface thermal conditions when remotely sensed data are employed, it may fail to address the human heat stress issue and associated factors, such as relative humidity. According to the results (Figure 22A, 22B and 22C), LST and DI were well correlated on 7/14 and 8/26 with R-squared values (all R squares are significant at 0.05 level in this study) of 0.99 and 0.98 respectively, which indicates that LST could be employed to indicate heat stress. However, R-squared suddenly dropped to zero on 8/6, which completely denied the conclusion drawn from 7/14 and 8/26. In order to verify this conflict, correlations among DI and NDVI and NDBI, which are two indicators of LST (Gallo, et al., 1993; Lo et al., 1997; Zha, et al., 2003), were also investigated in this study. Although R-squared values for NDVI and DI were higher than those for NDBI and DI, they varied following the same pattern of R-squared values for LST and DI, and dropped to zero for 8/6. As a vital factor which affects human comfort in warm environment, relative humidity was accounted for by using wet-bulb temperatures when DI was calculated. Thus, it was reasonable that the correlation between LST and DI was good when the spatial distribution of LST and wet-bulb temperature was similar (Figure 14A and 17A, Figure 14B and 17B), since the consistency of spatial distribution covered for LST failing to address the influence from relative humidity. However, when the spatial distributions of LST and wet-bulb temperature were dramatically different from each other (Figure 14C and 17C), the deficiency of LST surfaced. As relative humidity was considered, those areas with low LST values (Q_1) could still have high DI (Q_3) values, which indicated extreme discomfort due to the wet air. As a result, the correlation between LST and DI

57

dropped to zero on 8/6. This is consistent with temperatures of land surfaces not necessarily

deciding the feeling individuals experience. I believe this addressed the significance of DI as an

indicator which quantifies the actual heat stress individuals bear within warm environment. With

all these analyses and discussions completed, it is safe to claim that LST retrieved from remotely

sensed data is sufficient only as an indicator of surface UHI, as it fails to take air and humidity

information into account.

Addressing DI within continuous space may also help authorities better alleviate the damage

brought by heat waves. A lot of countries now have established heat wave plans to dictate

interventions when extreme hot days appear (Kovats and Hajat, 2008). Meteorological forecasts

are usually used to decide if the weather is hot enough to be a threat to public health, and where

the areas most seriously affected by heat waves will be. However, as it has been discussed in this

research, air temperature is not the only factor affecting heat stress. Humid days with lower air

temperature may lead to more heat stress than higher temperature days with dry air (Figure 16

and Figure 18). Thus, revealing DI with remotely sensed data within continuous space may

provide a reliable means to evaluate if the heat is sufficiently hazardous to public health to

warrant the intervention.
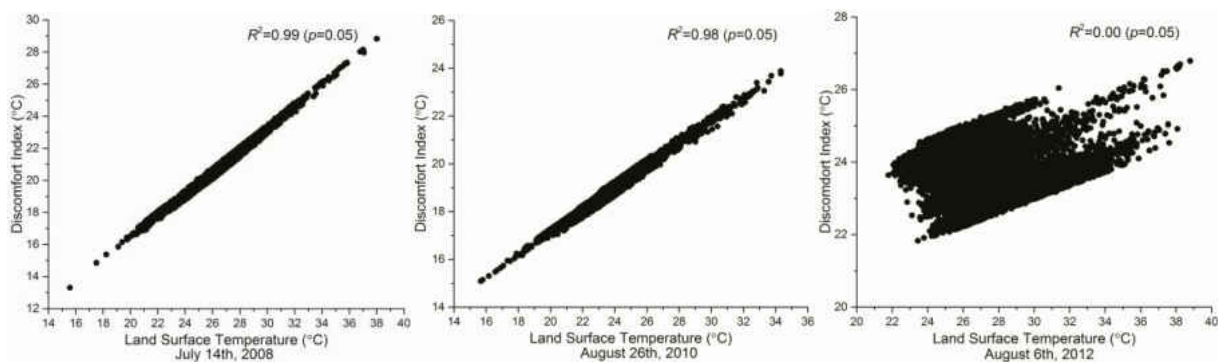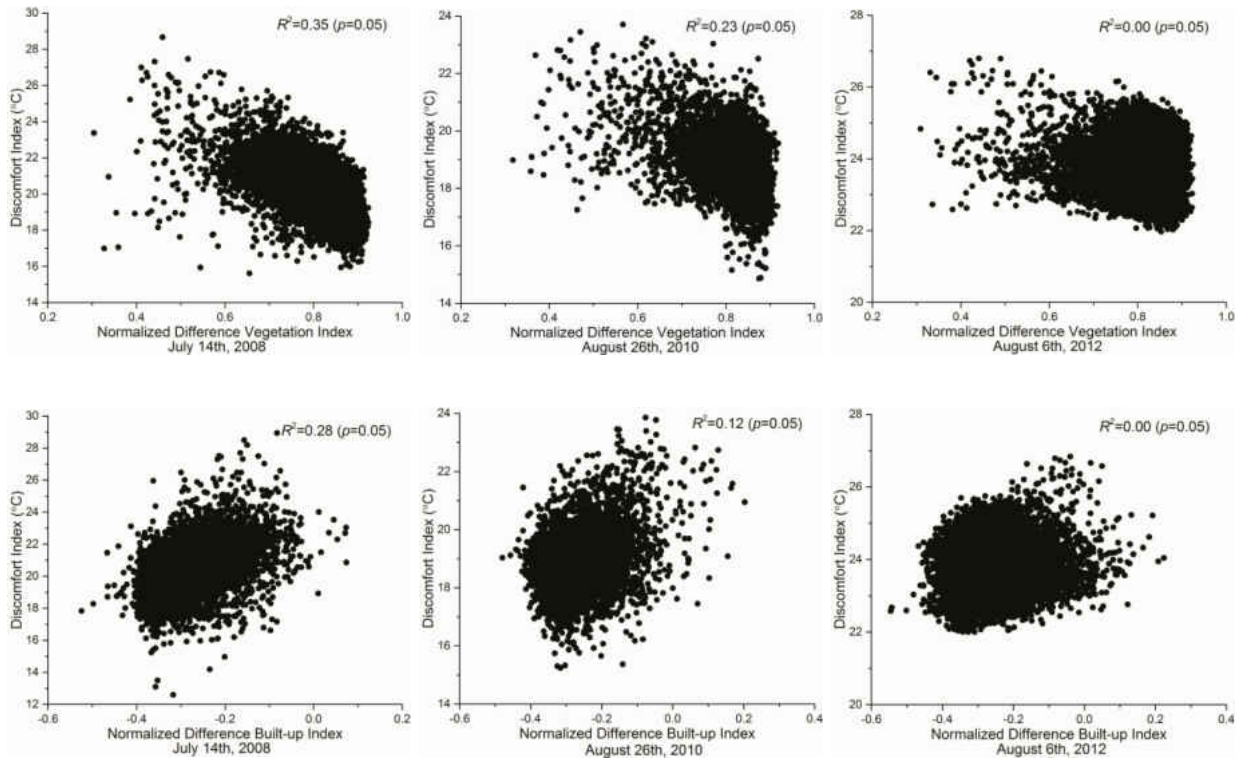
Figure 22 Correlation between DI and LST, NDVI and NDBI

3.6 Conclusion

This research focused on addressing of human heat stress through a perspective of continuous space and its implication for the administrative response to heat waves. The study began with retrieval of dry-bulb temperatures within the study area from weather-station- acquired air temperature and MODIS LST data for three summers. Results showed that air temperature calculated based on the three empirical models built in this research were fairly accurate with low RMSE values compared with existing studies. As DI was retrieved with the help of dry-bulb temperature and relative humidity, its spatial distribution within the study area was revealed for the selected days. Further investigation proved that relative humidity is the key factor that differentiates DI from LST, and influences the spatial distribution of DI. As LST does not take humidity into account when it is employed to address UHI, I believe DI is a better indicator

which addresses human discomfort when surrounded by a warm environment. Given what have been found in this study, I do realize the following limitations: (1) As intended to addressed heat stress with remotely sensed data, DI was retrieved due to its connection with LST. However, the accuracy of the retrieved DI is limited by the relatively complex retrieval process and the accuracy of LST; (2) Due to the limitation of resources, no field measurements were carried out in this study to evaluate the reliability of DI retrieved by the proposed method; and (3) All the results and conclusions drawn were based on one study area at a single scale. Future research in other areas at different scales should be done to verify the conclusions of this study.

CHAPTER 4 LANDSCAPE CONFIGURATION AND URBAN ENVIRONMENT: EXAMINING THE RELATIONSHIP BETWEEN LANDSCAPE CHARACTERISTICS AND HUMAN HEAT STRESS IN WISCONSIN, USA

4.1 Introduction

Urban heat island (UHI) refers to the phenomenon that urban area temperatures are usually higher than their surrounding rural areas, due to the urbanization associated atmospheric and surface modification (Voogt & Oke, 2003). Despite the urban-rural temperature difference, intra-urban temperature may also vary due to the modification of (1) urban land covers, such as the change in abundance of vegetation and impervious surfaces; (2) urban structure, such as the

height-width ratio of buildings; (3) urban fabric, such as the thermal property of asphalt and concrete; and (4) urban metabolism, such as energy discharged by human activities (Oke, 2006). Developed countries, such as the United States, have been experiencing rapid population growth and urban sprawl over the last three decades, and it is projected to continue (Alig et al., 2004). This trend may exacerbate the UHI through the feedbacks brought by urbanization. For example, changing of rural surfaces to urban surfaces (concrete, metal and asphalt etc.) leads to more thermal energy storage in urban areas and thus raises surface and air temperature. The warmer temperatures then results in more air conditioner use, indicating more energy consumption, which will again contribute to UHI (Landsberg, 1981). UHI influences the urban ecological environment and human well-being in negative ways (Connors et al., 2013). Take heat stress for instance, it appears as a health hazard when air temperature and humidity rise and leads to physical and phycological discomfort. Existing studies have reported increased emergency calls and hospital visits associated with heat waves (Kalkstein & Smoyer, 1993; Kinney et al., 2001). Vulnerability to heat stress depends on a population's sensitivity to heat environment and protection from heat stress, such as the availability of air conditioners and green space. As air conditioning systems are less affordable to lower income communities and residents therein usually face landscapes with less vegetation, low income urban citizens are in greater risk of heat stress. This poses not only a public health, but also an environmental justice issue with which policy makers and urban designers should be concerned.

UHI can be divided into three categories (Voogt & Oke, 2003): canopy layer heat island (CLHI), boundary layer heat island (BLHI) and surface urban heat island (SUHI). When remotely sensed data are employed to address UHI, SUHI is usually the target as remote sensors can only collect

61

surface spectral information. Within this realm, the relationship between land surface

temperature (LST) and land cover composition (proportion or abundance of a specific land cover

type within a specific region) has been well studied. For example, vegetation has been reported

to have the ability to cool its surrounding environment (Shashua-Bar & Hoffman, 2000).

Following this thought, the normalized difference vegetation index (NDVI) and vegetation

abundance have been proven to be negatively correlated with LST (Gallo et al., 1993; Lo et al.,

1997; Weng et al., 2004). Similarly, abundance of impervious surfaces has also been reported to

be positively correlated with LST (Yuan & Bauer, 2007). Other studies focus on the influence of

spatial configuration (or urban structure), such as the spatial arrangement and topographic

characteristics, of land cover patches within urban areas (Gustafson, 1998). Zhou et al. (2011)

examined the relationship between ten landscape metrics and LST in Maryland, USA and

compared it with land cover composition. Results indicate that land cover composition plays a

more significant role affecting LST than spatial configuration. Connors et al. (2013) classified

Phoenix, Arizona into three land uses (mesic residential, xeric residential and

commercial/industrial) and explored the connection between spatial configuration of typical land

covers (buildings, impervious and grass) and LST through ten landscape metrics at two levels

(class and landscape). Although Pearson's correlation coefficients indicate significant correlation

between some of these metrics and LST, it differs among land uses. Li et al. (2012) revealed the

spatial configuration of green space of Beijing and its relationship with LST. They found that

spatial configuration has significant impact of the variation of LST and increasing patch density

of green space leads to higher LST. Despite this previous work, LST is still the only indicator of

UHI when remotely sensed data are employed. However, heat stress is not only deermined by

surface temperature, but also by air temperature, humidity and physiological condition. When UHI afflicted human heat discomfort needs to be addressed, LST is insufficient as the indicator.

Quantifying heat stress has been a theme of public health research for decades. Many studies have been dedicated to estimating human heat stress originating from urban environments and climate with a heat stress index (Frank et al., 1996; Gonzalez et al., 1978; Wallace et al., 2005). Epstein and Moran (2006) classified these indices into three types, which are rationale indices, empirical indices and direct indices. While the first two groups of indices require both physiological and environmental input to calculate (and are thus beyond the scope of this research), direct indices are more straightforward to implement as only environmental variables (temperature and humidity etc.) are required as input. Wet-bulb globe temperature (WBGT) was developed by Yaglou and Minard (1957) to study the heat associated with injuries in US Navy training. Thom (1959) proposed a discomfort index (DI), which employs dry-bulb and wet-bulb temperature as input. Despite its simple form, DI has proven to be a reliable indicator of human heat stress, considering its correlation with ET and its physiological significance (Tennenbaum et al., 1961). As better indicators of human heat discomfort than LST, heat stress indices have mostly been measured and discussed in specific situations, such as military training grounds and construction sites. Their spatial distribution and relationship with land cover spatial configuration have barely been addressed.

In this research, I aim to investigate the influence of land cover spatial configuration on human heat stress. Specifically, objectives of this research include: (1) retrieval of DI with remotely sensed data to address human heat stress at the State level; (2) quantification of the spatial

configuration of typical land covers with selected landscape metrics; and (3) investigation of the

connection between human heat stress and spatial configuration of typical urban land covers. I

expect that better understanding of the influence of land cover structure on human heat stress can

support urban land cover planning and decisions regarding urban design which affects energy

consumption and human well-being.

4.2 Study area and data

The State of Wisconsin was selected as my study area for this research (Figure 23). With a

geographic area of 169,639 km^2, it is within the range of 42°37'N-47°5'N and 86°46'W-92°53'W.

Wisconsin has experienced dramatic urbanization during the last two decades. Population of the

state grew accordingly from 4.89 million of 1990 to 5.69 million in 2015, which is almost an

increase of 16% in 25 years. Further, temperatures in Wisconsin have also increased over the last

60 years (Human Health Working Group, 2011). As Wisconsin is expected to become

increasingly warmer, more urbanized and populated, UHI originated heat stress will have more

impact on people's lives in the future.

MODIS (Moderate-resolution Imaging Spectroradiometer) daytime LST (MOD11A1, daily LST

product with 1km spatial resolution) and precipitable water data (MOD07, atmospheric profile

product with 1km spatial resolution) for August 26th, 2010 (8/26) and August 6th, 2012 (8/6)

were obtained to retrieve saturated and actual vapor pressure respectively. MODIS land cover

type data (MCD12Q1, yearly land cover type product with 500m spatial resolution) for 2010 and

2012 were employed to identify typical land covers within the study area for spatial

configuration analysis. Air temperature and dew point temperature acquired on the selected days

from 49 meteorological stations distributed within the study area were also collected from

NOAA (National Oceanic and Atmospheric Administration) to calculate dry-bulb temperature,

vapor pressure and carry out associated accuracy assessment.
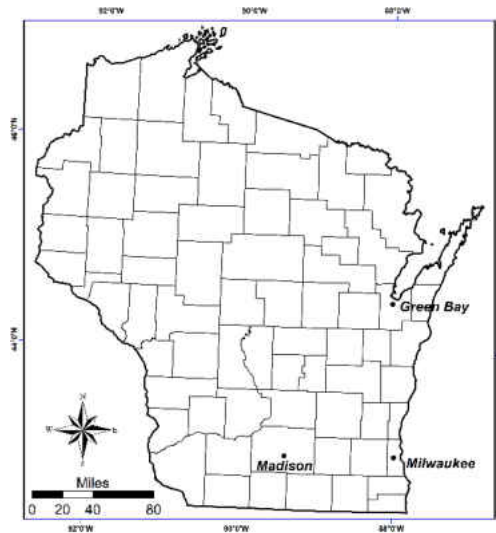
Figure 23 Study area

4.3 Methods

4.3.1 Retrieval of DI

DI was firstly designed by Thom (1959). Sohar et al. (1963) then adjusted it to the following

form:

$$DI = 0.5T_a + 0.5T_w \qquad (28)$$

where T_a (°C) is dry-bulb temperature; T_w (°C) is wet-bulb temperature. In order to retrieve DI,

dry-bulb temperature and wet-bulb temperature need to be retrieved first.

Dry-bulb Temperature

Dry-bulb temperature is defined as the air temperature acquired by a thermometer which is isolated from radiation and moisture, but exposed only to the air. In this research, air temperature retrieved from MODIS LST data was considered as dry-bulb temperature. Many studies have dedicated to investigate the relationship between air temperature and LST with remotely sensed data (Cresswell et al., 1999; Prihodko & Goward, 1997; Vancutsem et al., 2010). However, a widely accepted rationale model has not yet been proposed due to the complexity of the lowest atmospheric layers. Thus, two regional empirical models based on meteorological station-acquired data were established to address the connection between air temperature and LST. Air temperature of the selected days from 34 randomly selected NOAA meteorological stations were employed to build empirical models between air temperature and LST (Table 6). Air temperature from the remaining 15 stations available in the study area were utilized to calculate root mean square error (RMSE) for accuracy assessment of the models:

$$\text{RMSE} = \sqrt{\frac{1}{N}\sum_1^N (T_{a_i} - T_{a_i}')^2} \qquad\qquad (29)$$

where T_{a_i} is air temperature retrieved from LST; T_{a_i}' is the air temperature acquired by meteorological station i. N is the total number of meteorological station employed, which is 15 in this study.

Table 6 Models for dry-bulb temperature retrieval

Date	Model (°C)	R^2 ($p<0.05$)	RMSE (°C)
August 26th, 2010	Ta=1.29LST-2.21	0.62	0.86
August 06th, 2012	Ta=0.29LST+19.11	0.59	0.69

*Ta is dry-bulb temperature

Wet-bulb temperature

Wet-bulb temperature is defined as the temperature a parcel of air has when it is cooled to saturation while the parcel itself supplies the latent heat. As the measurement of wet-bulb temperature requires a thermometer wrapped in cloth wetted by distilled water, it is not practical to measure it within the study area with high spatial resolution. To overcome this obstacle, an empirical method proposed by Stull (2011) was utilized to retrieve wet-bulb temperature from relative humidity and air temperature. This method can be described through the following equation:

$$T_w = T_a * atan[0.151977(RH + 8.313659)^{0.5}] + atan(T_a + RH) - atan(RH - 1.676331) + 0.00391838 * RH^{1.5} * atan(0.023101RH) - 4.686035 \tag{30}$$

where T_a (°C) and T_w (°C) are dry-bulb and wet-bulb temperature respectively; RH (%) is relative humidity. Despite its validity, air pressure (kPa), air temperature (°C) and relative humidity (%) are required to be within a specific range to use it (Stull, 2011). Air temperature was between 18.06°C and 31.20°C, while RH was between 63.83% and 78.26% on the selected days. Both air temperature and RH were in the valid range. However, as the method is most accurate under standard atmospheric pressure (101.325kpa), the smaller the difference between actual air pressure and standard atmospheric pressure, the smaller the error is produced by the method. The air pressure of the study area varied between 95.4kpa and 99.7kpa for the selected days, and average values were 98.6kPa and 98.1kPa for 8/26 and 8/6 respectively. Since they were close to the ideal air pressure, it is reasonable to believe that the error is acceptable.

Relative humidity

Relative humidity can be defined by the following equation:

$$RH = \frac{e}{e_s} \tag{31}$$

where e (hpa) is vapor pressure and e_s (hpa) is saturated vapor pressure. In this research, e_s was calculated from air temperature through the Tetens equation:

$$e_s = 6.108 \times exp(\frac{17.27 \times T}{237.3 + T}) \tag{32}$$

where e_s (hpa) is saturated vapor pressure; T (°C) is the air temperature. Since the air temperature can be retrieved from LST, saturated vapor pressure was calculated across the study area with 1km spatial resolution. Further, although vapor pressure cannot be directly retrieved from remotely sensed data, existing studies have proven that precipitable water and vapor pressure are correlated linearly (Peng et al., 2007) or non-linearly (Karalis, 1974; Mori et al., 2017). Following this thought, vapor pressure for all meteorological stations on the selected days were first calculated from dew point temperature with the following formula:

$$e = 6.108 \times exp(\frac{17.27 \times T_d}{237.3 + T_d}) \tag{33}$$

where e (hpa) is vapor pressure; T_d (°C) is dew point temperature. As the relationship between precipitable water (MOD07) and vapor pressure from meteorological stations for the selected days were addressed with OLS regression, vapor pressure for the study area was retrieved utilizing the following model with 1km spatial resolution:

$$e = 7.087PW - 0.1736 \ (R^2 = 0.42, p < 0.05) \tag{34}$$

where e (hpa) is vapor pressure; PW (cm) is precipitable water. It is worth noting that only vapor pressure from 34 random selected stations were employed to build the model. Data from the

remaining 15 stations were utilized to do accuracy assessment as it was carried out for air temperature retrieval. RMSE of the model is 1.53hpa, which is 12% of the average vapor pressure from the 15 stations for accuracy assessment.

4.3.2 Spatial configuration of land covers

To address the spatial configuration of land covers within the study area, MODIS land cover type data (MCD12Q1) for 2010 and 2012 were employed. As MCD12Q1 provides land cover maps produced from 4 classification methods, I employed two maps for the selected days produced by MODIS-derived Net Primary Production (NPP) method. Specifically, each pixel is classified as one of the following land cover classes: water, urban, non-vegetated land, annual grass vegetation, evergreen needle-leaf vegetation, evergreen broadleaf vegetation, deciduous needle-leaf vegetation, deciduous broadleaf vegetation and annual broadleaf vegetation. However, I adjusted and introduced only 3 classes in this research: tree, grass and urban. There are several reasons for this rearrangement of land cover classes: (1) water was not selected since large water bodies in the study area are all natural, which means that even the relationship between their spatial configuration and heat stress is analyzed, they usually cannot be modified. Outdoor pools can barely be found due to local climate, and thus have no impact on the heat environment of the study area; (2) non-vegetated land was not selected since most of Wisconsin is covered by forests, grassland, cropland and urban areas. Large areas with bare soil may be found in winter when crops are harvested, but not in the selected summer days of this research; (3) all tree classes were combined as a single class as the cooling effect of different types of trees cannot be addressed separately and the selected days were in summer.

69

Given the location of the study area and spatial data resolution, I sampled 50 polygons from each

land cover map. Each patch is a square containing 11x11 pixels. To make samples

representative, a stratified random method was employed to ensure that half of the polygons are

from urban areas while the rest are from rural areas. For all the sampled polygons, I calculated 5

landscape metrics (Table 7) with FRAGSTATS software (McGarigal and Marks, 1995) at class

level to address the spatial configuration of different land cover types.

Table 7 List of landscape metrics employed in this research

Metric	Abbreviation	Description
Percent landscape	PLAND	Proportion of the total plot occupied by a given and cover class (percent)
Patch density	PD	Number of patches per hectare (number per hectare)
Edge density	ED	Sum of the length of all patch edges divided by the total area of the landscape (meters per hectare)
Landscape shape index	LSI	The total length of edge divided by the shortest possible edge length for the area of a patch (None)
Fractal dimension	FRAC_AM	A measure of departure from Euclidean geometry (none)

I then calculated Pearson's correlation coefficients using SPSS to assess the relationship between

each landscape metric and average DI of each sample patch (Table 8).

Table 8 Pearson's correlation coefficients between landscape metrics and DI

Metric	2010	2012
Tree		
PLAND	-0.737**	-0.459**
PD	0.352*	0.223
ED	-0.205	0.053
LSI	0.158	0.368**
FRAC_AM	-0.633**	-0.024
Urban		
PLAND	0.470**	0.499**
PD	0.410*	0.133
ED	0.447**	0.355*
LSI	0.439**	0.325*
FRAC_AM	0.239	0.443**
Grass		

PLAND	0.144	0.022
PD	0.094	0.114
ED	0.243	0.131
LSI	0.199	0.153
FRAC_AM	0.181	0.044

*$p<0.05$, ** $p<0.01$*

4.4 Results

4.4.1 LST and dry-bulb temperature

LST has been long been the indicator of surface UHI when remotely sensed data is employed to address urban environments. For 8/26 and 8/6, LST was between 18.54°C-35.83°C and 22.27°C-40.85°C, respectively. As indicated in Figure 24, populated areas, such as Milwaukee, Green Bay and Madison, were where high LST can be found. For most rural areas of Wisconsin, LST was lower than in urban areas. This spatial pattern is shown as scattered bright patches surrounded by large dark areas. Giving the contrast of LST that can be observed between rural and urban areas, surface UHI can be easily located for both years within metropolitan areas within the study area, especially Milwaukee and its surroundings. Dry-bulb temperature of the study area was considered equal to air temperature in this research, and was calculated from two regional empirical models established for the selected days (Figure 25). It varied between 18.06°C-26.46°C and 25.84°C-29.69°C on 7/14, 8/26 and 8/6, respectively. For the same location, dry-bulb temperature is usually lower than LST since thermal energy is easier to be stored in solid surface materials than air.
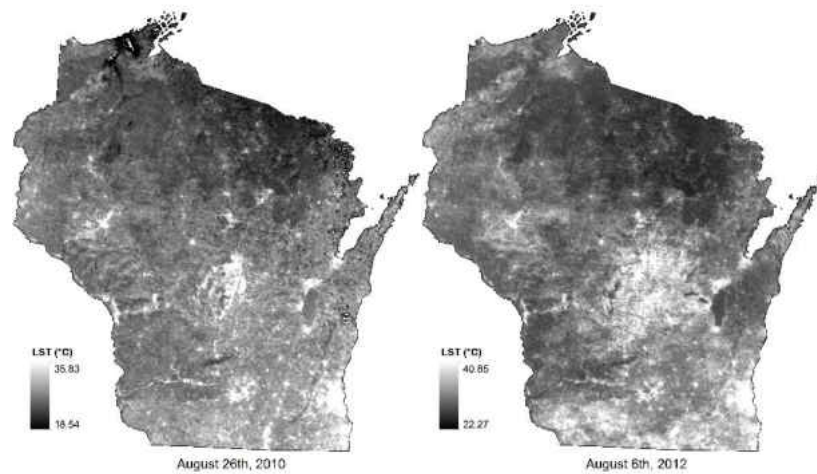
Figure 24 Spatial distribution of LST
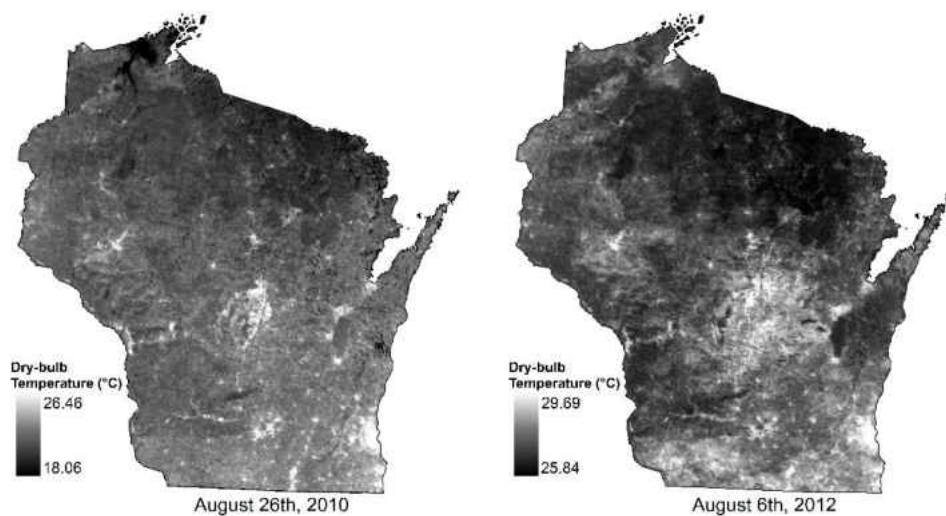
Figure 25 Spatial distribution of dry-bulb temperature

4.4.2 Wet-bulb temperature and DI

As another input of DI, wet-bulb temperature was calculated from dry-bulb temperature and RH (Figure 26). The spatial pattern of wet-bulb temperature (Figure 27) is similar for the selected days: (1) high wet-bulb temperature is shown as bright pixels and can be found in urban sites

scattered within the study area. Shoreline locations on Lake Michigan were also found to have

high wet-bulb temperature; (2) mid-northern parts of the State, which are mostly covered by

vegetation and small water bodies, were with low wet-bulb temperatures for both selected days;

(3) southern half of the study area generally had higher wet-bulb temperatures as the distance to

Lake Michigan is small and most urban areas of the state are clustered in south. Despite the

similar spatial distribution, wet-bulb temperatures varied between 12.07°C-16.34°C and

15.95°C-19.04°C on 8/26 and 8/6 respectively. DI was eventually calculated as the weighted

sum of dry-bulb and wet-bulb temperature, and varied between 15.24°C-19.97°C and 20.94°C-

24.01°C for the selected days (Figure 28). To guide the use of DI as a measurement of human

heat stress, Epstein and Moran (2006) developed criteria to address the severity of heat stress

(Table 9). Following these criteria, heat stress for most of the study area was level 1 and level 2,

which indicates no heat stress and mild heat stress.
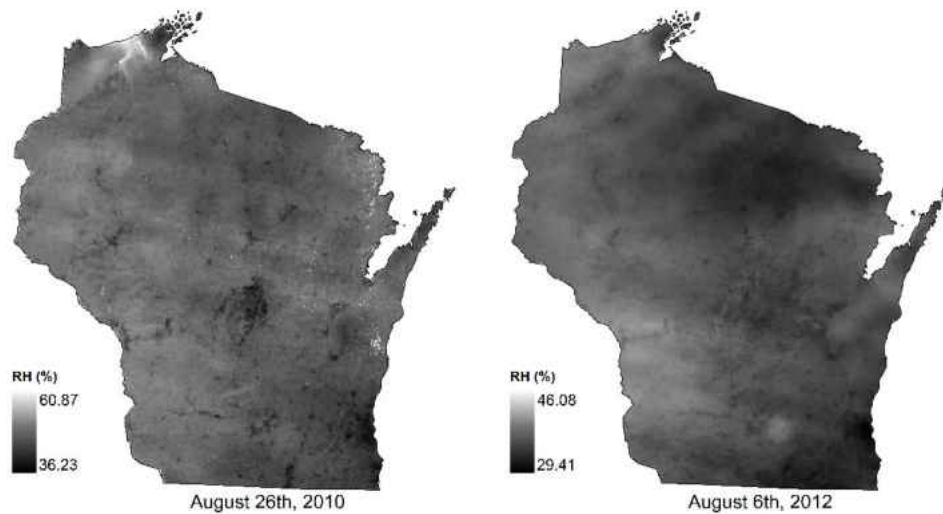
Figure 26 Spatial distribution of relative humidity
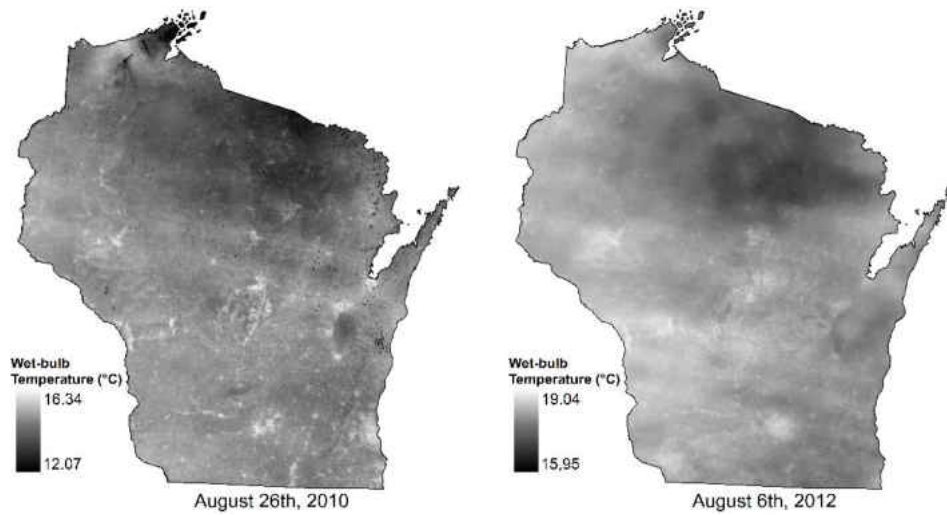
Figure 27 Spatial distribution of wet-bulb temperature

Spatial distribution of DI is similar to that of LST : (1) bright pixels, which represent high DI

values, were found in populated urban regions, especially around big cities such as Milwaukee,

Madison and Green Bay; (2) low DI values were found among rural areas surrounding urbanized

areas; (3) mid-northern part of the study area is special with only a scattering of very small towns

and is mostly covered by vegetation, which led to a clear boundary between this region and the

rest of the State as DI of this part was dramatically low.

Table 9 Ranking system for human heat stress

Rank	Range	Description
Level 1	DI ≤ 22°C	No heat stress can be sensed
Level 2	22°C < DI ≤ 24°C	Mild heat stress can be sensed
Level 3	24°C < DI ≤ 28°C	Moderate heat stress can be sensed
Level 4	DI > 28°C	Severe heat stress can be sensed
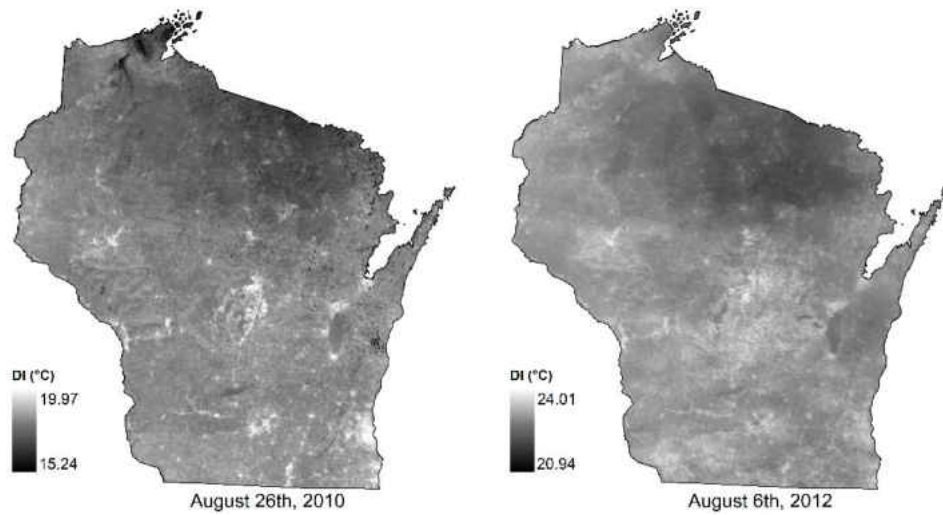
Figure 28 Spatial distribution of DI

4.4.3 Correlation between DI and landscape metrics

Pearson correlation coefficients (r) indicated that the relationship between DI and landscape metrics is different among three classes (Table 8). For tree class, PLAND were negatively correlated with DI for both 8/26 (r=-0.737, p<0.01) and 8/6 (r=-0.459, p<0.01) as they cool the surrounding environment through evapotranspiration and shades of tree canopies. PD (r=0.352, p<0.05) and FARC_AM (r=-0.633, p<0.01) were positively and negatively correlated with DI for only 8/26, while LSI (r=0.368, p<0.01) was positively correlated with DI for 8/6. Specifically, positive correlation between PD and DI indicates that when the total area of trees is settled, arranging them in numerous small patches would aggravate heat stress while less but bigger tree patches help alleviating it. LSI and FRAC_AM address the aggregation and complexity of a patch, respectively. Their implication on the spatial configuration of tree class will be discussed in the next section. Urban class showed strong positive correlation with DI through different landscape metrics. PLAND (r=0.470, p<0.01; r=0.499, p<0.01), ED (r=0.447,

p<0.01; *r*=0.355, *p*<0.05) and LSI (*r*=0.439, *p*<0.01; *r*=0.325, *p*<0.05) were significantly correlated with DI for both selected days. On the other hand, PD (*r*=0.410, *p*<0.05) and FRAC_AM (*r*=0.443, *p*<0.01) were only significantly correlated with DI for 8/26 and 8/6 respectively. As expected, PLAND of urban class was positively correlated with DI as widely distributed impervious surfaces are the main origin of excessive thermal energy stored in urban areas. FRAC_AM and ED of urban class were both positively correlated with DI, which is opposite to the correlation between them for tree class. Grass is unique compared to the rest two classes. Although all metrics have positive Pearson's *r*, none of them were significantly correlated with DI for both selected days, which indicates that spatial configuration of grass has positive but insignificant influence on human heat stress. This is opposite to the well-accepted opinions on the relationship between grass and UHI effect. More discussion regarding this conflict can be found in the next section.

4.5 Discussion

Dry-bulb and wet-bulb temperature are two inputs for DI. With proper equipment, their measurement is not difficult when DI is required at specific locations. However, calculating DI at State scale with high spatial resolution makes the measurement of dry-bulb and wet-bulb temperature a challenging task. In this research, I retrieved dry-bulb temperature by building empirical models realting air temperature and LST. Empirical models between vapor pressure and precipitable water were also built to calculate RH. Then wet-bulb temperature was retrieved from RH and dry-bulb temperature. Regional empirical models were accurate for the selected days within the study area, and helped retrieving DI. However, as a tradeoff, since it is impossible to carry out field measurement within the study area with high resolution, method

76

employed to retrieve DI in this research have their drawbacks. First, empirical models only expressed the statistical relationship between independent and dependent variables and failed to address the rationale beyond the statistical analysis. Second, as empirical models were all built based on the data (from meteorological stations and MODIS) collected at specific time, their availability is exclusive for the short time windows when data were collected, and thus should not be applied to any other scenarios. Last but not the least, the proposed method to retrieve wet-bulb temperature is very sensitive to data errors. Retrieval of wet-bulb temperature requires dry-bulb temperature and vapor pressure, which were not directly measured but also retrieved from LST and precipitable water. This means that errors produced during the measurement of LST and precipitable water will be amplified through the two-step retrieving process of wet-bulb temperature. Thus, quality of MOD11A1 (LST) and MOD07 (precipitable water) has a vital impact on the reliability of retrieved DI.

The revealed spatial pattern of DI was expected, as DI is the linear combination of dry-bulb and wet-bulb temperature. In my research, these two inputs were retrieved from LST and RH. Specifically, RH (Figure 26) of the selected days varied in relatively narrow ranges and distributed evenly within the study area, thus had very limited impact on the spatial pattern when RH was utilized to calculate wet-bulb temperature and eventually DI. As a result, the spatial distribution of wet-bulb and DI were similar to LST since RH of the selected days was stable within the study area. This argument is supported by previous research which also chose August 6th, 2012 for DI retrieval but with a different RH data source (Song and Wu, 2017). In that research, RH data was acquired directly from North America Regional Reanalysis (NARR). RH from NARR varied in a much larger range and its spatial distribution was different from RH

retrieved in this research. Similarly, the spatial distribution of DI was also dramatically different

due to the influence from RH. I would not like to argue whether RH acquired from NARR or

retrieved from precipitable water is more accurate as the data source and retrieval method are

both reliable. However, the impact of RH on DI should be emphasized through the spatial

inconsistency of DI for the same day.

Pearson's correlation coefficients provided some results that were expected, but also some that

surprised me (Table 8). LSI represents the aggregation of a class. For trees, low LSI indicates a

patch with a compact shape while high LSI means a less aggregated patch containing dispersed

trees. The positive correlation between LSI and DI on 8/6 suggests that tree patches with more

compact shapes would benefit more for alleviating heat stress. FRAC_AM is an indicator of

shape complexity. The higher the FRAC_AM, the more convoluted a patch is. The negative

Pearson's correlation coefficient between FRAC_AM and DI on 8/26 indicates that tree patches

with complex shapes tend to lower DI. This can be explained by the extent of the interface

between vegetation and its surrounding environment. Studies regarding vegetation's impact on

UHI have confirmed that the cooling effect of vegetation is mainly controlled by several factors,

including the extent of interface between vegetation and surrounding areas (Alexandri and Jones

2008; Bowler et al. 2010; Ca et al. 1998; Oliveira et al. 2011; Onishi et al. 2010; Qiu et al. 2013).

As the complexity of a tree patch increases, the edge of the patch also increases, which leads to a

larger patch-surrounding interface and enhancement of the patch's cooling effect. This also

indicates that when the area of trees is decided, the interface between trees and surrounding

environment expands as more small patches appear (high PD), and thus should lead to a stronger

cooling effect and less heat stress (lower DI). It is interesting that the interface theory here

seemingly conflicts with the result that PD and DI are positively correlated. The positive

correlation between PD and DI implicates that aggregating trees in one big patch is better than

planting them in scattered small patches in terms of the alleviation of heat stress. However, I

believe this seeming conflict does not mean the nonviability of the interface theory but the result

of a tradeoff, as the benefit brought by the aggregation of trees exceeds the drawbacks of the

decreased interface when larger patches are made.

For grass class, Pearson's correlation coefficients between landscape metrics and DI were all

positive but statistically insignificant for both days. This result surprised me since grass has been

proven as an alleviator of surface UHI in previous studies (Imhoff et al., 2010; Weng et al.,

2004), and it was expected to have negative impact on heat stress. Despite the unexpected

results, I believe the conflict between the output of this research and existing studies can be

explained. Grass as a type of vegetation can lower the temperature of surrounding environment.

However, as it exists near the ground, its cooling effect is weaker than trees and limited to the

ground surface. Thus, it is reasonable that grass has negative impact on LST, but not on DI. On

the other hand, since grass cannot provide shades, standing on the grass indicates direct exposure

to sunlight, which contributes to higher heat stress. This may explain why the Pearson's

correlation coefficient between PLAND and DI was positive. As for the remaining landscape

metrics (PD, ED, LSI and FRAC_AM), although their correlation with DI were all weak and

insignificant, results still indicates that fewer grass patches with simple shapes would alleviate

heat stress.

As rural landscapes become fragmented and heterogeneous during urbanization, spatial complexity of land covers also increases (Wu et al., 2011; York et al., 2011). Although the change of spatial structure and its influence on urban heat environment has been discussed (Brazel et al., 2000; Buyantuyev & Wu, 2010), its relationship with human heat stress remains untouched. As the comfort of urban environment has been more emphasized during the rapid urbanization at global scale, implications on the relationship between spatial configuration and urban heat stress could be beneficial to policy-makers. Optimizing land cover spatial configuration enables policy-makers to balance the usage of energy, water and social resources, and effectively manage urban mosaics. Based on the results of this research, creating more complex and long-edge tree patches would benefit the alleviation of heat stress, while simple and compact urban patches would minimize the heat stress brought by impervious surfaces.

4.6 Conclusion

Urbanization comes with the alteration of land covers, which has been a driver of local climate change (Quattrochi & Ridd, 1994). Expanding urban areas leads to the UHI effect, which has implications for human health. This research not only revealed human heat stress at the State level with remotely sensed data, but also addressed the connection between spatial configuration of land covers and DI. As expected, PLAND of trees and impervious surfaces were negatively and positively correlated with DI, similar to their connections with LST. Correlation analysis for other landscape metrics indicated that land covers can also affect DI through their spatial configuration. The presented research also overturned the established perspective on grass, which has been well accepted as an alleviator of LST. Results indicated that the spatial arrangement of grass has limited impact on DI, and larger area of grass may lead to even more

80

heat stress. Findings of this research have important implications for land cover planning. In order to reduce heat stress, policy makers and urban designers should take spatial configuration of land covers into account. Despite the results, I also realize the limitations to overcome in future: (1) this research was carried out at only the mesoscale. Effectiveness of conclusion drawn from the research should be validated at other scales, especially at microscale where the spatial configuration of land cover is more complex; (2) climate context was not considered in this research. As Wisconsin has a typical temperate climate, areas with arid and tropical climate should be considered in the future to validate if the conclusion drawn here is climate-dependent; and (3) due to financial limitations, no field measurements were done to assess the accuracy of retrieved DI across the study area.

CHAPTER 5 CONCLUSION

5.1 Summary

With the rapid urbanization around the world, urban heat islands (UHI), as a byproduct of human activities, have become a key issue which affects urban climate, ecology, and human health. Research on UHI have long been carried out with both traditional ground-based observations and remotely sensed data to support the decision-making process of policy makers and city planners. However, despite the continuous endeavor of understanding UHI phenomena, there are still challenging problems yet to be solved. Specifically, neighboring effect has barely been addressed when remotely sensed data is employed to study UHI. Ignoring the potential influence from surrounding environments may lead to a biased estimation of land surface temperature (LST). Moreover, although human heat stress brought by UHI has been studied for more than a century,

it is usually measured at scattered indiviudual sites, and has never been addressed in a continuous space at a large scale. Therefore, this research employed multiple data types, including remotely sensed and ground collected data, to achieve the following purposes: (1) investigate the influence of neighboring environment on LST variation; (2) propose two methods to retrieve DI at mesoscale and (3) explore its correlation with land cover composition and configuration. Specifically, a moving window method was utilized to address the impact of neighboring environment on the retrieval of LST. NARR relative humidity data, MODIS atmospheric profile data and MODIS LST data were then combined to retrieve discomfort index at the State level. Finally, the correlation between DI and land cover composition and configuration was investigated to provide implications for land cover planning.

5.2 Contributions

The first contribution of the research is addressing of neighboring effect through the moving window method. LST has long been utilized as the indicator of surface UHI when remotely sensed data are employed to study urban environments. However, each pixel is usually treated as an isolated object when LST is retrieved, which neglects that LST of a pixel can be affect by its surrounding environment. As the neighboring effect is neglected, more deviation from a true value is brought into the retrieved LST. To account for the influence of neighboring environment, a moving window method was proposed for a better estimation of LST. Statistical analysis proved that the correlation between %ISA and LST improves when neighboring effect is considered. Moreover, while accounting for neighboring effect leads to a better estimation of LST, definition of neighboring environment is vital. An undersized area may fail to include all

neighboring pixels that can impact the central pixel, while an oversized area covers pixels that has no thermal influence on the central one.

The second contribution of the research lies in the retrieval of human heat stress with remotely sensed data. Heat stress is an environmental hazard which can seriously affect productivity, health or even survival of individuals, and has long been studied. Despite the efforts that have been made to address the issue quantitatively with various heat stress indices, they are often measured at only scattered individual sites. Further, while remotely sensed data can be utilized to reveal UHI within continuous space, LST as the widely used indicator is incapable of addressing human heat stress, as it simply represents surface thermal conditions. Other factors affecting human comfort, such as air temperature and relative humidity cannot be addressed by LST. To bridge the gap, two methods were proposed in this research to retrieve DI at the State scale with remotely sensed data. As both methods successfully revealed DI at fine spatial resolution, the difference between them lies in the retrieval of wet-bulb temperature. The retrieval of DI with remotely sensed data indicates that relative humidity is the main factor that affects the spatial distribution of DI. And since LST as an indicator of surface UHI does not consider humidity, DI is a better indicator of human heat stress when remotely sensed data are utilized to study UHI.

The third contribution of the research is exploring the relationship between DI and land cover composition and configuration. The correlation between DI and land cover composition indicates that abundance of vegetation and impervious surfaces is negatively and positively correlated with DI, respectively. This makes sense since impervious surfaces are usually considered as the source of UHI while vegetation is the alleviator of UHI due to the evapotranspiration. However,

this relationship is not permanent. When the spatial distribution of relative humidity changes dramatically, the correlation between DI and land cover composition could disappear. Further, the spatial configuration aspect of the relationship between DI and land cover (trees, urban and grass) is more complex. For trees, while large patches help alleviate heat stress, patches with complex shapes are also welcome. For urban areas, large patches can also be helpful for alleviating heat stress, but patches with complex shapes are not encouraged. Spatial configuration of grass unexpectedly has no significant impact on DI. The possible reason is that although it cools the surrounding environment, it does not provide shade and the cooling effect only benefits surface areas and thus has very limited ability to make people feel cooler. Research on the relationship between DI and land cover configuration expands the understanding of the impact of land cover configuration on heat stress by quantifying spatial structure of land covers. It may also provide insights for policy makers and urban designers on mitigating hazardous environmental effects brought by urbanization.

5.3 Future research

Future research will focus on the following aspects. First, current results of the research need to be verified at different scales. Both the investigation of neighboring effect and the retrieval of DI, have been done in this research at only a single scale – at county or State level. While the modifiable areal unit problem (MAUP) (Jelinski and Wu, 1996) indicates that conclusions drawn at one scale can be incorrect at another one, it is important to extend the current research to multiple scales for verification. Second, climate context should be considered in the future to better understand the spatial variation of DI. Air temperature and relative humidity are crucial to the retrieval of DI. However, they were only statistically calculated from remotely sensed and

weather station data in this research. A better understanding of their variation from a perspective of climatology would help find out if there is relationship between the spatial pattern of DI and specific climate types. Third, as DI reveals human heat stress from a perspective of the physical environment, socio-economic factors such as poverty level, median house income, ethnicity, age and heat sensitive illness can also affect, directly or indirectly, the actual heat stress perceived by individuals. Thus, socio-economic factors should be introduced to the future research to form a more comprehensive understanding of human heat stress, which provides administrations at different levels practical information for better management of heat stress related issues during the warm season.

REFERENCES

Ackerman, B. (1985). Temporal march of the Chicago heat island. Journal of Climate and Applied Meteorology, 24(6), 547-554.

Adams, J. B., Sabol, D. E., Kapos, V., Almeida Filho, R., Roberts, D. A., Smith, M. O., & Gillespie, A. R. (1995). Classification of multispectral images based on fractions of endmembers: Application to land-cover change in the Brazilian Amazon. Remote sensing of Environment, 52(2), 137-154.

Alexandri, E., & Jones, P. (2008). Temperature decreases in an urban canyon due to green walls and green roofs in diverse climates. Building and Environment, 43(4), 480-493.

Alig, R. J., Kline, J. D., & Lichtenstein, M. (2004). Urbanization on the US landscape: looking ahead in the 21st century. Landscape and urban planning, 69(2), 219-234.

Amiri, R., Weng, Q., Alimohammadi, A., & Alavipanah, S. K. (2009). Spatial–temporal dynamics of land surface temperature in relation to fractional vegetation cover and land use/cover in the Tabriz urban area, Iran. Remote sensing of environment, 113(12), 2606-2617.

Asrar, G., Fuchs, M., Kanemasu, E. T., & Hatfield, J. L. (1984). Estimating absorbed photosynthetic radiation and leaf area index from spectral reflectance in wheat. Agronomy journal, 76(2), 300-306.

Avissar, R. (1996). Potential effects of vegetation on the urban thermal environment. Atmospheric Environment, 30(3), 437-448.

Bacci, L., Morabito, M., Raschi, A., & Ugolini, F. (2003). Thermohygrometric conditions of some urban parks of Florence (Italy) and their effects on human well-being. trees, 6, 49.

Balaras, C., Tselepidaki, I., Santamouris, M., & Asimakopoulos, D. (1993). Calculations and statistical analysis of the environmental cooling power index for Athens, Greece. Energy conversion and management, 34(2), 139-146.

Barradas, V. L. (1991). Air temperature and humidity and human comfort index of some city parks of Mexico City. International Journal of Biometeorology,35(1), 24-28.

Barsi, J. A., Schott, J. R., Palluconi, F. D., & Hook, S. J. (2005, July). Validation of a web-based atmospheric correction tool for single thermal band instruments. In Proc. SPIE (Vol. 5882, pp. 136-142).

Becker, F., & Li, Z. L. (1990). Towards a local split window method over land surfaces. Remote Sensing, 11(3), 369-393.

Belding, H. S., & Hatch, T. F. (1955). Index for evaluating heat stress in terms of resulting physiological strain. Heating, piping and air conditioning, 27(8), 129.

Bell, P. A. (1981). Physiological, comfort, performance, and social effects of heat stress. Journal of Social Issues, 37(1), 71-94.

Ben-Dor, E., & Saaroni, H. (1997). Airborne video thermal radiometry as a tool for monitoring microscale structures of the urban heat island. International Journal of Remote Sensing, 18(14), 3039-3053.

Black, A., & Stephen, H. (2014). Relating temperature trends to the normalized difference vegetation index in Las Vegas. GIScience & remote sensing, 51(4), 468-482.

Bobb, J. F., Peng, R. D., Bell, M. L., & Dominici, F. (2014). Heat-related mortality and adaptation to heat in the United States. Environmental health perspectives, 122(8), 811.

Bowler, D. E., Buyung-Ali, L., Knight, T. M., & Pullin, A. S. (2010). Urban greening to cool towns and cities: A systematic review of the empirical evidence. Landscape and urban planning, 97(3), 147-155.

Brazel, A., Selover, N., Vose, R., & Heisler, G. (2000). The tale of two climates—Baltimore and Phoenix urban LTER sites. Climate Research, 15(2), 123-135.

Buyantuyev, A., & Wu, J. (2010). Urban heat islands and landscape heterogeneity: linking spatiotemporal variations in surface temperatures to land-cover and socioeconomic patterns. Landscape ecology, 25(1), 17-33.

Carlson, T. N., Gillies, R. R., & Perry, E. M. (1994). A method to make use of thermal infrared temperature and NDVI measurements to infer surface soil water content and fractional vegetation cover. Remote Sensing Reviews, 9(1-2), 161-173.

Ca, V. T., Asaeda, T., & Abu, E. M. (1998). Reductions in air conditioning energy caused by a nearby park. Energy and Buildings, 29(1), 83-92.

Cetin, M., Adiguzel, F., Kaya, O., & Sahap, A. (2016). Mapping of bioclimatic comfort for potential planning using GIS in Aydin. Environment, Development and Sustainability, 1-15.

Cetin, M. (2015). Determining the bioclimatic comfort in Kastamonu City. Environmental monitoring and assessment, 187(10), 640.

Chang, C. R., Li, M. H., & Chang, S. D. (2007). A preliminary study on the local cool-island intensity of Taipei city parks. Landscape and Urban Planning, 80(4), 386-395.

Connors, J. P., Galletti, C. S., & Chow, W. T. (2013). Landscape configuration and urban heat island effects: assessing the relationship between landscape characteristics and land surface temperature in Phoenix, Arizona. Landscape ecology, 28(2), 271-283.

Cresswell, M. P., Morse, A. P., Thomson, M. C., & Connor, S. J. (1999). Estimating surface air temperatures, from Meteosat land surface temperatures, using an empirical solar zenith angle model. International Journal of Remote Sensing, 20(6), 1125-1132.

Cristóbal, J., Ninyerola, M., & Pons, X. (2008). Modeling air temperature through a combination of remote sensing and GIS data. Journal of Geophysical Research: Atmospheres (1984–2012), 113(D13).

Dash, P., Göttsche, F. M., Olesen, F. S., & Fischer, H. (2002). Land surface temperature and emissivity estimation from passive sensor data: theory and practice-current trends. International Journal of remote sensing, 23(13), 2563-2594.

Deng, C., & Wu, C. (2012). BCI: A biophysical composition index for remote sensing of urban environments. Remote Sensing of Environment, 127, 247-259.

Dufton, A. F. (1929). The eupatheostat. Journal of scientific instruments, 6(8), 249.

Epstein, Y., Keren, G., Moisseiev, J., Gasko, O., & Yachin, S. (1980). Psychomotor deterioration during exposure to heat. Aviation, space, and environmental medicine, 51(6), 607-610.

Epstein, Y., & Moran, D. S. (2006). Thermal comfort and the heat stress indices. Industrial health, 44(3), 388-398.

Eyre, A. (1982). Arid Zone Settlement Planning: The Israeli Experience. 223-226.

Frank, A., Moran, D., Epstein, Y., Belokopytov, M., & Shapiro, Y. (1996). The estimation of heat tolerance by a new cumulative heat strain index. Environmental Ergonomics: Recent Progress and New Frontiers, eds Shapiro Y., Moran D., Epstein Y.(Freund, London), 194-197.

Gallo, K. P., McNab, A. L., Karl, T. R., Brown, J. F., Hood, J. J., & Tarpley, J. D. (1993). The use of NOAA AVHRR data for assessment of the urban heat island effect. Journal of Applied Meteorology, 32(5), 899-908.

Gallo, K. P., & Owen, T. W. (1999). Satellite-based adjustments for the urban heat island temperature bias. Journal of Applied Meteorology, 38(6), 806-813.

Georgi, N. J., & Zafiriadis, K. (2006). The impact of park trees on microclimate in urban areas. Urban Ecosystems, 9(3), 195-209.

Gill, S. (2006). Climate change and urban greenspace (Doctoral dissertation, The University of Manchester).

Givoni, B. (1991). Impact of planted areas on urban environmental quality: a review. Atmospheric Environment. Part B. Urban Atmosphere, 25(3), 289-299.

Golden, J. S., Carlson, J., Kaloush, K. E., & Phelan, P. (2007). A comparative study of the thermal and radiative impacts of photovoltaic canopies on pavement surface temperatures. Solar Energy, 81(7), 872-883.

Gonzalez, R. R., Berglund, L. G., & Gagge, A. P. (1978). Indices of thermoregulatory strain for moderate exercise in the heat. Journal of Applied Physiology, 44(6), 889-899.

Grimmond, C. S. B., & Oke, T. R. (1991). An evapotranspiration-interception model for urban areas. Water Resources Research, 27(7), 1739-1755.

Gustafson, E. J. (1998). Quantifying landscape spatial pattern: what is the state of the art?. Ecosystems, 1(2), 143-156.

Hafner, J., & Kidder, S. Q. (1999). Urban heat island modeling in conjunction with satellite-derived surface/soil parameters. Journal of applied meteorology, 38(4), 448-465.

Haldane, J. S. (1905). The Influence of High Air Temperatures No. I. Journal of Hygiene, 5(04), 494-513.

Hao, P., Niu, Z., Zhan, Y., Wu, Y., Wang, L., & Liu, Y. (2016). Spatiotemporal changes of urban impervious surface area and land surface temperature in Beijing from 1990 to 2014. GIScience & Remote Sensing, 53(1), 63-84.

Harazono, Y., Teraoka, S., Nakase, I., & Ikeda, H. (1991). Effects of rooftop vegetation using artificial substrates on the urban climate and the thermal load of buildings. Energy and buildings, 15(3), 435-442.

Heusinkveld, B. G., Van Hove, L. W. A., Jacobs, C. M. J., Steeneveld, G. J., Elbers, J. A., Moors, E. J., & Holtslag, A. A. M. (2010, April). Use of a mobile platform for assessing urban heat stress in Rotterdam. In Proceedings of the 7th Conference on Biometeorology (Vol. 12).

Hien, W. N., Yok, T. P., & Yu, C. (2007). Study of thermal performance of extensive rooftop greenery systems in the tropical climate. Building and Environment, 42(1), 25-54.

Hill, L., Griffith, O. W., & Flack, M. (1916). The measurement of the rate of heat-loss at body temperature by convection, radiation, and evaporation.Philosophical Transactions of the Royal Society of London. Series B, Containing Papers of a Biological Character, 183-220.

Hondula, D. M., Balling, R. C., Vanos, J. K., & Georgescu, M. (2015). Rising temperatures, human health, and the role of adaptation. Current Climate Change Reports, 1(3), 144-154.

Höppe, P. (2002). Different aspects of assessing indoor and outdoor thermal comfort. Energy and buildings, 34(6), 661-665.

Houghton, F. C., & Yaglou, C. P. (1923). Determining equal comfort lines. J ASHVE, 29, 165-176.

Huang, L., Li, J., Zhao, D., & Zhu, J. (2008). A fieldwork study on the diurnal changes of urban microclimate in four types of ground cover and urban heat island of Nanjing, China. Building and environment, 43(1), 7-17.

Human Health Working Group. (2011). Wisconsin Initiative on Climate Change Impacts. Human Health Working Group Report, 48.

Imhoff, M. L., Zhang, P., Wolfe, R. E., & Bounoua, L. (2010). Remote sensing of the urban heat island effect across biomes in the continental USA. Remote sensing of environment, 114(3), 504-513.

Irish, R. R. (2000). Landsat 7 science data user's handbook. National Aeronautics and Space Administration, Report, 430-15.

Jauregui, E. (1991). Influence of a large urban park on temperature and convective precipitation in a tropical city. Energy and buildings, 15(3), 457-463.

Jelinski, D. E., & Wu, J. (1996). The modifiable areal unit problem and implications for landscape ecology. Landscape ecology, 11(3), 129-140.

Jiménez-Muñoz, J. C., & Sobrino, J. A. (2003). A generalized single-channel method for retrieving land surface temperature from remote sensing data.Journal of Geophysical Research: Atmospheres (1984–2012), 108(D22).

Kalkstein, L. S., & Smoyer, K. E. (1993). The impact of climate change on human health: some international implications. Cellular and molecular life sciences, 49(11), 969-979.

Karalis, J. D. (1974). Precipitable water and its relationship to surface dew point and vapor pressure in Athens. Journal of Applied Meteorology, 13(7), 760-766.

Kauth, R. J., & Thomas, G. S. (1976, January). The tasselled cap--a graphic description of the spectral-temporal development of agricultural crops as seen by Landsat. In LARS Symposia (p. 159).

Kinney, P., Shindell, D., Chae, E., & Winston, B. (2001). Climate change and public health: Impact assessment for the NYC metropolitan region. 2001 Climate Change and a Global City: An Assessment of the Metropolitan East Coast Region, 103-147

Kjelgren, R., & Montague, T. (1998). Urban tree transpiration over turf and asphalt surfaces. Atmospheric Environment, 32(1), 35-41.

Kloog, I., Chudnovsky, A., Koutrakis, P., & Schwartz, J. (2012). Temporal and spatial assessments of minimum air temperature using satellite surface temperature measurements in Massachusetts, USA. Science of the Total Environment, 432, 85-92.

Kolokotsa, D., Psomas, A., & Karapidakis, E. (2009). Urban heat island in southern Europe: The case study of Hania, Crete. Solar Energy, 83(10), 1871-1883.

Landsberg, H. E. (1981). The urban climate (Vol. 28). National Academic Press, New York.

Li, J., Song, C., Cao, L., Zhu, F., Meng, X., & Wu, J. (2011). Impacts of landscape structure on surface urban heat islands: a case study of Shanghai, China. Remote Sensing of Environment, 115(12), 3249-3263.

Lind, A. R., & Hellon, R. F. (1957). Assessment of physiological severity of hot climates. Journal of applied physiology, 11(1), 35-40.

Li, X., Zhou, W., Ouyang, Z., Xu, W., & Zheng, H. (2012). Spatial pattern of greenspace affects land surface temperature: evidence from the heavily urbanized Beijing metropolitan area, China. Landscape ecology, 27(6), 887-898.

Lo, C. P., Quattrochi, D. A., & Luvall, J. C. (1997). Application of high-resolution thermal infrared remote sensing and GIS to assess the urban heat island effect. International Journal of Remote Sensing, 18(2), 287-304.

Markham, B. L., & Barker, J. L. (1986). Landsat MSS and TM post-calibration dynamic ranges, exoatmospheric reflectances and at-satellite temperatures. EOSAT Landsat Technical Notes, No. 1.

McGarigal, K., & Marks, B. J. (1995). Spatial pattern analysis program for quantifying landscape structure. Gen. Tech. Rep. PNW-GTR-351. US Department of Agriculture, Forest Service, Pacific Northwest Research Station.

McKarns, J. S., & Brief, R. S. (1966). Nomographs Give Refined Estimate of Heat Stress Index. Journal of Occupational and Environmental Medicine, 8(10), 557.

McMichael, A. J., Woodruff, R. E., & Hales, S. (2006). Climate change and human health: present and future risks. The Lancet, 367(9513), 859-869.

Meehl, G. A., & Tebaldi, C. (2004). More intense, more frequent, and longer lasting heat waves in the 21st century. Science, 305(5686), 994-997.

Moran, D. S., Pandolf, K. B., Shapiro, Y., Heled, Y., Shani, Y., Mathew, W. T., & Gonzalez, R. R. (2001). An environmental stress index (ESI) as a substitute for the wet bulb globe temperature (WBGT). Journal of thermal biology, 26(4), 427-431.

Moran, D. S., Shitzer, A., & Pandolf, K. B. (1998). A physiological strain index to evaluate heat stress. American Journal of Physiology-Regulatory, Integrative and Comparative Physiology, 275(1), R129-R134.

Mori, M., Nojima, T., & Sai, K. (2017). A quasi-linear relationship between GPS-derived precipitable water vapor and surface vapor pressure observed on dry days in spring and autumn: a case study at Saga Plain in northern Kyushu Island, Japan. Paddy and Water Environment, 15(2), 425-432.

Mueller, E. C., & Day, T. A. (2005). The effect of urban ground cover on microclimate, growth and leaf gas exchange of oleander in Phoenix, Arizona.International Journal of Biometeorology, 49(4), 244-255.

Munn, R. E., Hirt, M. S., & Findlay, B. F. (1969). A climatological study of the urban temperature anomaly in the lakeshore environment at Toronto. Journal of Applied Meteorology, 8(3), 411-422.

Myrup, L. O. (1969). A numerical model of the urban heat island. Journal of Applied Meteorology, 8(6), 908-918.

Nunez, M., & Oke, T. R. (1980). Modeling the daytime urban surface energy balance. Geographical Analysis, 12(4), 373-386.

Oke, T. R. (1989, November). CHARACTERIZATION OF URBAN HEAT ISLANDS. In Proceedings of the Workshop on Saving Energy and Reducing Atmospheric Pollution by (p. 7). Okwen, R. T., Pu, R., & Cunningham, J. A. (2011). Remote sensing of temperature variations around major power plants as point sources of heat. International Journal of Remote Sensing, 32(13), 3791–3805.

Oke, T. R. (2006). Instruments and observing methods: Report No. 81: initial guidance to obtain representative meteorological observations at urban sites. World Meteorological Organization, WMO/TD (1250).

Oliveira, S., Andrade, H., & Vaz, T. (2011). The cooling effect of green spaces as a contribution to the mitigation of urban heat: A case study in Lisbon.Building and Environment, 46(11), 2186-2194.

Onishi, A., Cao, X., Ito, T., Shi, F., & Imura, H. (2010). Evaluating the potential for urban heat-island mitigation by greening parking lots. Urban forestry & Urban greening, 9(4), 323-332.

Pachauri, R. K., Allen, M. R., Barros, V. R., Broome, J., Cramer, W., Christ, R., ... & Dubash, N. K. (2014). Climate change 2014: synthesis report. Contribution of Working Groups I, II and III to the fifth assessment report of the Intergovernmental Panel on Climate Change (p. 151). IPCC.

Palluconi, F. D., & Meeks, G. R. (1985). Thermal Infrared Multispectral Scanner (TIMS): an investigator's guide to TIMS data.

Patz, J. A., Campbell-Lendrum, D., Holloway, T., & Foley, J. A. (2005). Impact of regional climate change on human health. Nature, 438(7066), 310-317.

Peng, G. X., Li, J., Chen, Y. H., & Norizan, A. P. (2007). A method of estimating relative humidity from MODIS atmospheric profile products. J. Trop. Meteor, 23(6), 611-616

Price, J. C. (1984). Land surface temperature measurements from the split window channels of the NOAA 7 Advanced Very High Resolution Radiometer.Journal of Geophysical Research: Atmospheres (1984–2012), 89(D5), 7231-7237.

Prihodko, L., & Goward, S. N. (1997). Estimation of air temperature from remotely sensed surface observations. Remote Sensing of Environment, 60(3), 335-346.

Qin, Z. H., Karnieli, A., & Berliner, P. (2001). A mono-window algorithm for retrieving land surface temperature from Landsat TM data and its application to the Israel-Egypt border region. International Journal of Remote Sensing, 22(18), 3719-3746.

Qiu, G. Y., LI, H. Y., Zhang, Q. T., Wan, C. H. E. N., Liang, X. J., & Li, X. Z. (2013). Effects of evapotranspiration on mitigation of urban temperature by vegetation and urban agriculture. Journal of Integrative Agriculture, 12(8), 1307-1315.

Quattrochi, D. A., & Ridd, M. K. (1994). Measurement and analysis of thermal energy responses from discrete urban surfaces using remote sensing data. International Journal of Remote Sensing, 15(10), 1991-2022.

Rashed, T., Weeks, J. R., Roberts, D., Rogan, J., & Powell, R. (2003). Measuring the physical composition of urban morphology using multiple endmember spectral mixture models. Photogrammetric Engineering & Remote Sensing, 69(9), 1011-1020.

Rhee, J., Park, S., & Lu, Z. (2014). Relationship between land cover patterns and surface temperature in urban areas. GIScience & remote sensing, 51(5), 521-536.

Ridd, M. K. (1995). Exploring a VIS (vegetation-impervious surface-soil) model for urban ecosystem analysis through remote sensing: comparative anatomy for cities†. International Journal of Remote Sensing, 16(12), 2165-2185.

Roberts, D. A., Gardner, M., Church, R., Ustin, S., Scheer, G., & Green, R. O. (1998). Mapping chaparral in the Santa Monica Mountains using multiple endmember spectral mixture models. Remote Sensing of Environment, 65(3), 267-279.

Robine, J. M., Cheung, S. L. K., Le Roy, S., Van Oyen, H., Griffiths, C., Michel, J. P., & Herrmann, F. R. (2008). Death toll exceeded 70,000 in Europe during the summer of 2003. Comptes rendus biologies, 331(2), 171-178.

Semenza, J. C., Rubin, C. H., Falter, K. H., Selanikio, J. D., Flanders, W. D., Howe, H. L., & Wilhelm, J. L. (1996). Heat-related deaths during the July 1995 heat wave in Chicago. New England journal of medicine, 335(2), 84-90.

Schmugge, T., Hook, S. J., & Coll, C. (1998). Recovering surface temperature and emissivity from thermal infrared multispectral data. Remote Sensing of Environment, 65(2), 121-131.

Shapiro, Y., & Seidman, D. S. (1990). Field and clinical observations of exertional heat stroke patients. Medicine and science in sports and exercise, 22(1), 6-14.

Shashua-Bar, L., & Hoffman, M. E. (2000). Vegetation as a climatic component in the design of an urban street: An empirical model for predicting the cooling effect of urban green areas with trees. Energy and Buildings, 31(3), 221-235.

Sheridan, S. C., & Kalkstein, L. S. (2004). Progress in heat watch–warning system technology. Bulletin of the American Meteorological Society, 85(12), 1931-1941.

Shi, L., Liu, P., Kloog, I., Lee, M., Kosheleva, A., & Schwartz, J. (2016). Estimating daily air temperature across the Southeastern United States using high-resolution satellite data: A statistical modeling study. Environmental research, 146, 51-58.

Small, C. (2001). Estimation of urban vegetation abundance by spectral mixture analysis. International journal of remote sensing, 22(7), 1305-1334.

Smith, M. O., Johnson, P. E., & Adams, J. B. (1985). Quantitative determination of mineral types and abundances from reflectance spectra using principal components analysis. Journal of Geophysical Research: Solid Earth (1978–2012), 90(S02), C797-C804.

Snyder, W. C., Wan, Z., Zhang, Y., & Feng, Y. Z. (1998). Classification-based emissivity for land surface temperature measurement from space. International Journal of Remote Sensing, 19(14), 2753-2774.

Sobrino, J. A., Caselles, V., & Becker, F. (1990). Significance of the remotely sensed thermal infrared measurements obtained over a citrus orchard. ISPRS Photogrammetric Engineering and Remote Sensing, 44, 343–354.

Sobrino, J. A., Raissouni, N., & Li, Z. -L. (2001). A comparative study of land surface emissivity retrieval from NOAA data. Remote Sensing of Environment, 75, 256–266.

Sobrino, J., Coll, C., & Caselles, V. (1991). Atmospheric correction for land surface temperature using NOAA-11 AVHRR channels 4 and 5. Remote sensing of environment, 38(1), 19-34.

Stoll, M. J., & Brazel, A. J. (1992). Surface-air temperature relationships in the urban environment of Phoenix, Arizona. Physical Geography, 13(2), 160-179.

Sohar, E., Adar, R., & Kaly, J. (1963). Comparison of the environmental heat load in various parts of Israel. Bull Res Counc Israel E, 10, 111-5.

Spronken-Smith, R. A., & Oke, T. R. (1998). The thermal regime of urban parks in two cities with different summer climates. International journal of remote sensing, 19(11), 2085-2104.

Steeneveld, G. J., Koopmans, S., Heusinkveld, B. G., Van Hove, L. W. A., & Holtslag, A. A. M. (2011). Quantifying urban heat island effects and human comfort for cities of variable size and urban morphology in the Netherlands.Journal of Geophysical Research: Atmospheres (1984–2012), 116(D20).

Streiling, S., & Matzarakis, A. (2003). Influence of single and small clusters of trees on the bioclimate of a city: a case study. Journal of Arboriculture, 29(6), 309-316.

Stull, R. (2011). Wet-bulb temperature from relative humidity and air temperature. Journal of Applied Meteorology and Climatology, 50(11), 2267-2269.

Souch, C. A., & Souch, C. (1993). The effect of trees on summertime below canopy urban climates. Journal of Arboriculture, 19, 303-303.

Southeastern Wisconsin Regional Planning Commission (2004a). The population of Southeastern Wisconsin, technical report #11 (4th ed.). Available online at:http://www.sewrpc.org/SEWRPCFiles/publications/techrep/tr-011_population_southeastern_wisconsin.pdf (assessed on May 26, 2012).

Southeastern Wisconsin Regional Planning Commission (2004b). The Economy of Southeastern Wisconsin, technical report #10 (4th ed.). Available online at:http://www.sewrpc.org/SEWRPCFiles/Publications/TechRep/tr-010_economy_southeastern_wisconsin.pdf(assessed on May 26, 2012).

Southeastern Wisconsin Regional Planning Commission (2010). Census Population and Household Counts: 1980-2010.

Spronken-Smith, R. A., & Oke, T. R. (1998). The thermal regime of urban parks in two cities with different summer climates. International journal of remote sensing, 19(11), 2085-2104.

Taha, H., Akbari, H., & Rosenfeld, A. (1991). Heat island and oasis effects of vegetative canopies: micro-meteorological field-measurements. Theoretical and Applied Climatology, 44(2), 123-138.

Takebayashi, H., & Moriyama, M. (2007). Surface heat budget on green roof and high reflection roof for mitigation of urban heat island. Building and Environment, 42(8), 2971-2979.

Tennenbaum, J., Sohar, E., Adar, R., & Gilat, T. (1961). The Physiological Significance of the Cumulative Discomfort Index (Cum. DI). Harefuah, 60(10), 315-19.

Thom, E. C. (1959). The discomfort index. Weatherwise, 12(2), 57-61.

Tou, J. T., & Gonzalez, R. C. (1974). Pattern recognition principles.

United Nations, Department of Economic and Social Affairs, Population Division (2012). World Urbanization Prospects, the 2011 Revision: Highlights. New York: United Nations.

Upmanis, H., Eliasson, I., & Lindqvist, S. (1998). The influence of green areas on nocturnal temperatures in a high latitude city (Göteborg, Sweden).International journal of climatology, 18(6), 681-700.

U.S. Census Bureau (2010). Census, American FactFinder. (2010). Available online at: http://factfinder2.census.gov/

Vancutsem, C., Ceccato, P., Dinku, T., & Connor, S. J. (2010). Evaluation of MODIS land surface temperature data to estimate air temperature in different ecosystems over Africa. Remote Sensing of Environment, 114(2), 449-465.

Van Der Meer, F., & De Jong, S. M. (2000). Improving the results of spectral unmixing of Landsat Thematic Mapper imagery by enhancing the orthogonality of end-members. International Journal of Remote Sensing, 21(15), 2781-2797.

Vernon, H. M., & Warner, C. G. (1932). The influence of the humidity of the air on capacity for work at high temperatures. Journal of Hygiene, 32(03), 431-462.

Voogt, J. A., & Oke, T. R. (2003). Thermal remote sensing of urban climates. Remote sensing of environment, 86(3), 370-384.

Wallace, R. F., Kriebel, D. A. V. I. D., Punnett, L. A. U. R. A., Wegman, D. H., Wenger, C. B., Gardner, J. W., & Gonzalez, R. R. (2005). The effects of continuous hot weather training on risk of exertional heat illness. Medicine and science in sports and exercise, 37(1), 84-90.

Weng, Q. (2001). A remote sensing? GIS evaluation of urban expansion and its impact on surface temperature in the Zhujiang Delta, China. International journal of remote sensing, 22(10), 1999-2014.

Weng, Q., Lu, D., & Schubring, J. (2004). Estimation of land surface temperature–vegetation abundance relationship for urban heat island studies.Remote sensing of Environment, 89(4), 467-483.

Wong, N. H., Chen, Y., Ong, C. L., & Sia, A. (2003). Investigation of thermal benefits of rooftop garden in the tropical environment. Building and environment, 38(2), 261-270.

Wu, C., & Murray, A. T. (2003). Estimating impervious surface distribution by spectral mixture analysis. Remote sensing of Environment, 84(4), 493-505.

Wu, J., Jenerette, G. D., Buyantuyev, A., & Redman, C. L. (2011). Quantifying spatiotemporal patterns of urbanization: The case of the two fastest growing metropolitan regions in the United States. Ecological Complexity, 8(1), 1-8.

Yaglou, C. P., & Minard, D. (1957). Control of heat casualties at military training centers. AMA Archives of Industrial Health, 16(4), 302.

Yilmaz, H., Toy, S., Irmak, M. A., Yilmaz, S., & Bulut, Y. (2008). Determination of temperature differences between asphalt concrete, soil and grass surfaces of the City of Erzurum, Turkey. Atmósfera, 21(2), 135-146.

York, A. M., Shrestha, M., Boone, C. G., Zhang, S., Harrington, J. A., Prebyl, T. J., ... & Wright, J. B. (2011). Land fragmentation under rapid urbanization: A cross-site analysis of Southwestern cities. Urban Ecosystems, 14(3), 429-455.

Yuan, F., & Bauer, M. E. (2007). Comparison of impervious surface area and normalized difference vegetation index as indicators of surface urban heat island effects in Landsat imagery. Remote Sensing of Environment, 106(3), 375-386.

Yue, W., Xu, J., Tan, W., & Xu, L. (2007). The relationship between land surface temperature and NDVI with remote sensing: application to Shanghai Landsat 7 ETM+ data. International Journal of Remote Sensing, 28(15), 3205-3226.

Yu, C., & Hien, W. N. (2006). Thermal benefits of city parks. Energy and Buildings, 38(2), 105-120.

Zha, Y., Gao, J., & Ni, S. (2003). Use of normalized difference built-up index in automatically mapping urban areas from TM imagery. International Journal of Remote Sensing, 24(3), 583-594.

Zhou, W., Huang, G., & Cadenasso, M. L. (2011). Does spatial configuration matter? Understanding the effects of land cover pattern on land surface temperature in urban landscapes. Landscape and Urban Planning, 102(1), 54-63.

CURRICULUM VITAE

EDUCATION

2018 (Expected) **Ph.D. Geography, University of Wisconsin-Milwaukee, USA**
Dissertation title: *Examining Human Heat Stress with Remote Sensing Technologies*
Advisor: Dr. Changshan Wu

2012 **M.S. Cartography and Geographic Information Science, University of Chinese Academy of Sciences, China**
Thesis title: *Research on Absorption Properties of Urban Water Bodies in Beijing*
Advisor: Dr. Bing Zhang

2008 **B.S. Measurement and Control Technology and Instrument, Beijing University of Chemical Technology, China**

RESEARCH INTERESTS

- Geographic information science
- Geospatial analysis
- Remote sensing
- Cartography
- Public health

PUBLICATIONS

Peer-reviewed journal articles:

2016 **Song, Y.**, & Wu, C. (2016). Examining the Impact of Urban Biophysical Composition and Neighboring Environment on Surface Urban Heat Island Effect. *Advances in Space Research*, *57*(1), 96-109.

2017 **Song, Y.**, & Wu, C. (2017). Examining human heat stress with remote sensing technology. GIScience & Remote Sensing, 1-19.

2017 **Song, Y.**, & Wu, C. Landscape configuration and urban environment: examining the relationship between landscape characteristics and human heat stress in Wisconsin, USA *Under review.*

PRESENTATIONS

Conference presentations

2016 Yang Song. Retrieving Discomfort Index with Remotely Sensed Data. *Annual Meeting of the Association of American Geographers*, San Francisco, CA, March 29 - April2.

2014 Yang Song. Spectral Absorption Features of Particulate Matter and Colored Dissolved Organic Matter in Beijing Olympic Lake. *Annual Meeting of the Association of American Geographers*, Tampa, FL, April 8-12.

TEACHING EXPERIENCE

2016-2017   **Lab Instructor and discussion leader**, Department of Geography, UWM

            Fall: GEOG 247: Quantitative Analysis in Geography
                     GEOG 600: Perspectives on Geography

2015-2016   **Instructor, lab Instructor and discussion leader**, Department of Geography, UWM

            Fall: GEOG 247: Quantitative Analysis in Geography
                     GEOG 600: Perspectives on Geography
            Spring: GEOG 405: Cartography (Instructor)

2014-2015   **Lab Instructor and discussion leader**, Department of Geography, UWM

            Fall: GEOG 625: Intermediate Geographic Information Science
                     GEOG 110: The World: Peoples and Regions
            Spring: GEOG 405: Cartography

2013-2014   **Lab Instructor**, Department of Geography, UWM
            Fall: GEOG 547: Spatial Analysis
            Spring: GEOG 405: Cartography
                     GEOG 525: Geographic Information Science

2012-2013   **Discussion facilitator**, Department of Geography, UWM
            Fall: GEOG 110: The World: Peoples and Regions
            Spring: GEOG 110: The World: Peoples and Regions

PROFESSIONAL MEMBERSHIPS

2013-Present   Association of American Geographers (AAG)
2013-Present   Student Chapter of ASPRS at UWM
2014-Present   GIS Club at UWM

HONORS AND AWARDS

2016-2017   Mary Jo Read Fellowship, Department of Geography, UWM
2016   Mary Jo Read Travel Award, Department of Geography, UWM
2016   First Place, Student GIS Project Competition, GIS Council, UWM
2015-2016   Mary Jo Read Fellowship, Department of Geography, UWM
2014   Mary Jo Read Travel Award, Department of Geography, UWM
2013-2014   Mary Jo Read Fellowship, Department of Geography, UWM
2012-2013   Chancellor's Graduate Student Award, UWM

PROFESSIONAL SKILLS

- Software packages: ArcGIS, QGIS, GeoDa, ERDAS, ENVI, eCognition
Programing language: R, Python, Matlab